Università degli studi di Bergamo
Facoltà di Ingegneria
Dipartimento di Ingegneria Industriale

Dottorato in Tecnologie per l'Energia e l'Ambiente
XX ciclo

DESIGN AND SIMULATION OF SOLAR ABSORPTION COOLING SYSTEMS

Giovanni Nurzia

Supervisor:
Prof. Antonio Perdichizzi

Bergamo, February 2008

Acknowledgements

I would like to express my deep gratitude to Prof. Antonio Perdichizzi, who has guided me through this work and during my PhD candidature. Together with him, other persons at the Department of Industrial Engineering have given me advises, suggestions and support. Among them I would like to name Ing. Giuseppe Franchini and Prof. Giovanna Barigozzi.

A part of this thesis was thought and written at the Technische Universität of Berlin. This has been possible thanks to the willingness of Prof. Felix Ziegler and the support of Ing. Jan Albers. I went to Berlin with many questions and I got back to Italy with answers and new interesting questions. The inspiring discussions I had with Prof. Ziegler and Ing. Albers have always given me the right insight into problems.
I would also like to thank Ing. Stefan Petersen, who encouraged me to stay in Berlin and allowed me to be part of his family.

Finally I wish to acknowledge the encouragement received from my colleagues and my family. They have been a constant example of love for knowledge and confidence in science.

Abstract

The aim of this work is to improve the modeling of single stage absorption chillers and to asses a design procedure for solar cooling systems based on computer simulations.
The absorption technology is reviewed in its fundamentals, with an effort on the phenomena that might be considered or not in a physical model.
A basic version of the absorption chiller model, which assumes that the heat transfer characteristics of the standard components do not depend on working conditions, is applied to simulate generic commercial chillers. The procedure outlined requires the knowledge of the nominal working condition of the chiller, a data which is usually available from manufacturers. The model applied to the simulation of a chiller produced by the Thermax company shows good agreement with the off design curves declared by the manufacturer.
The hypotheses of this basic model are then reviewed, in order to catch some important aspects in the simulation of the Yazaki WFC-10 chiller. It is the first attempt, and therefore susceptible of improvement, to model the entire Yazaki chiller taking into account the behaviour of its heat exchangers. A compromise between theoretical modeling and experimental correlations has been adopted, due to the complexity of the chiller and its barely accessible patented design. Some encouraging results have been obtained, but they point out that further research on the heat and mass transfer phenomena in the Yazaki absorption chiller is needed.

The absorption chiller modeling is then exploited in a computer tool that gives valuable information on the planning of solar cooling systems. The design of these systems involves the choice of the main components, their sizing and an adequate control strategy of the whole. Several installations are present worldwide, but there is a lack of standard planning methodology. In the present thesis the focus is on the choice of the plant elements and their sizing. Energy savings and economic competitiveness are regarded as essential in guiding the design process.
To find out an ideal sizing of the system the optimization-simulation approach is introduced. Once a typical system layout is chosen the TRNSYS environment is employed to see how different sizes of the

system components effect the overall energy performance. The main design variables considered are the orientation of the solar collector array, the collectors area, the nominal capacity of the absorption chiller, the nominal capacity of the back up compression chiller, the volume of the thermal storages. Several simulations are launched by an external optimization programme, that retrieves the value of an objective function and changes the variables consequently.
The procedure has been applied to a real planning case, carried out in two different installation sites. The results show that the economic convenience of solar cooling systems is really not easy going in the present scenario. Primary energy savings and reduction of electrical peak loads during hot season are more like to push the spread of this technology in the next future.

Finally a section of the present work describes how the absorption cycle model can be exploited to design a novel chiller. The allocation of the heat transfer area among the standard components of a chiller is analysed to get the best compromise between cost and thermodynamic performance. The geometry of each exchanger is optimized looking for a trade off between primary cost of the tubes and running cost of the pump employed in the external circuits.

Symbol	*Definition*	*Unit*
A	total heat transfer area	m^2
CF	cash flow	€
COP	coefficient of performance	dimensionless
D	diameter	m
f	friction factor	dimensionless
F	fouling factor	$m^2\ K\ W^{-1}$
g	gravitational acceleration	$m\ s^{-2}$
h	specific enthalpy	$J\ kg^{-1}$
h_i, h_o	heat transfer coefficient for inner and outer flow respectively	$W\ m^{-2}\ K^{-1}$
k	thermal conductivity	$W\ m^{-1}\ K^{-1}$
L	length	m
Nu	Nusselt number	dimensionless
p	pressure	Pa
Pr	Prandtl number	dimensionless
PW	present worth	€
Q	heat transfer rate	W
Re	Reynolds number	dimensionless
S	cost function	€
T	temperature, internal stream	°C
t	temperature, external stream	°C
U	overall heat transfer coefficient	$W\ m^{-2}\ K^{-1}$
x	solution concentration, weight percent of LiBr in water	%
Z	cost	€

Greek symbols		
α	heat transfer coefficient	W m^{-2} K^{-1}
Γ	mass flow rate per wetted perimeter	kg m^{-1} s^{-1}
δ	film thickness	m
ΔT	temperature difference	°C
η	efficiency	dimensionless
μ	dynamic viscosity	N s m^{-2}
ρ	density	kg m^{-3}
Subscripts		
A	absorber	
abs	absorption chiller	
b	boiler	
C	condenser	
c	cold	
Coll	solar collectors	
comp	compression	
conv	conventional	
cool	cooling	
E	evaporator	
el	electrical	
fr	fraction	
G	generator	
h	hot	

i	inner
l	liquid
L	thermal load
lm	logarithmic mean
max	maximum
nom	nominal
o	outer
OPC	operating cost
r	refrigerant
R	regenerative
s	strong solution
sat	saturation
sol	solution
st	thermal storage
tower	cooling tower
w	weak solution

1 The absorption chiller process

1.1 Ideal absorption chiller process

A single stage absorption chiller is essentially a three temperatures device. It removes a quantity of heat Q_E from a source at low temperature T_E, it rejects a quantity of heat Q_M to a source with a temperature close to the environment T_M, it is driven by a quantity of heat Q_G taken from a source at high temperature T_G. The quantity of heat Q_E is the refrigeration capacity of the chiller.

A diagram of this ideal device is shown in Figure 1.1. The three heat sources are considered to be large enough such that any heat input or output does not change their temperature. In the case of perfect heat transfer, three portions of the chiller have the same temperatures T_E, T_M and T_G of the heat sources.

Moreover, considering an ideal case, all the processes within the chiller are reversible.

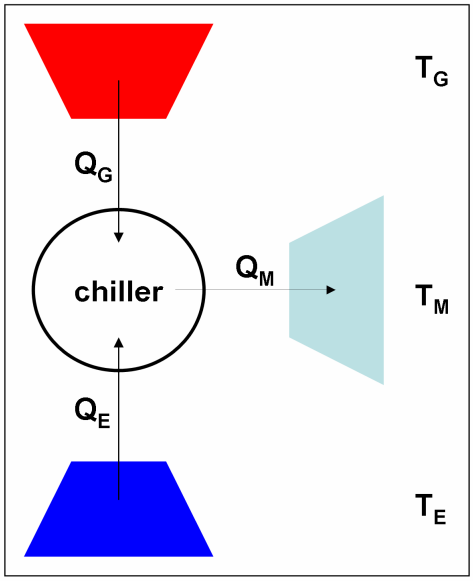

Figure 1.1 Ideal absorption chiller exchanging heat with three heat reservoirs

To analyze the steady state operation of the chiller it is sufficient to apply the 1st and the 2nd law of thermodynamic.
The 1st law gives:

$$Q_E + Q_G = Q_M \tag{1.1}$$

The general form of the 2nd law would be:

$$\Delta S = \Delta S_s + \sum_i \frac{Q_i}{T_i} \tag{1.2}$$

For a system in steady state the change in entropy ΔS over any time step is equal to zero. For the chiller considered, because all the internal processes are said to be reversible, also the entropy creation due to irreversibility ΔS_s is equal to zero. So the (1.1) reduces to:

$$\sum_i \frac{Q_i}{T_i} = \frac{Q_E}{T_E} + \frac{Q_G}{T_G} - \frac{Q_M}{T_M} = 0 \tag{1.3}$$

Inserting the (1.1) in the (1.3) and rearranging leads to:

$$Q_G \frac{T_G - T_M}{T_G} = Q_E \frac{T_M - T_E}{T_E} \tag{1.4}$$

The left hand side of the (1.4) is the work performed by a Carnot cycle operating between the temperatures T_G and T_M, while the right hand side is the work supplied to a Carnot cycle operating between the temperatures T_M and T_E.
The combination of the two aforementioned Carnot cycles gives the ideal absorption cycle. This can be represented in a T – s diagram as illustrated in Figure 1.2.

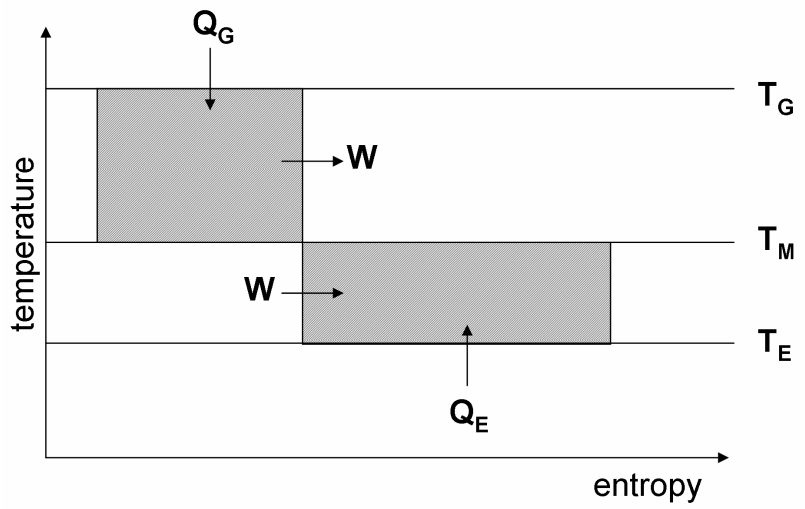

Figure 1.2 Ideal absorption chiller as the combination of two Carnot cycles

The global effect of the two cycles is to remove a quantity of heat Q_E at low temperature, at the expense of a quantity of heat Q_G taken at high temperature. Each of the cycle rejects a certain amount of the total heat Q_M at the temperature T_M. The quantity of work W is equal for the two cycles, as stated by the (1.4) and as shown by the two equal dashed areas in Figure 1.2.
To define the efficiency of a refrigerating cycle the ratio between the useful cooling effect and the energy spent to obtain it can be used. In the present case this ratio is given by:

$$COP_{ideal} = \frac{Q_E}{Q_G} = \frac{T_E}{T_G}\frac{(T_G - T_M)}{(T_M - T_E)} \tag{1.5}$$

From the (1.5) it is a simple matter to see how the COP_{ideal} changes with the three temperatures: it increases for increasing T_E and T_G, while it decreases for increasing T_M.
This behavior can be shown qualitatively also on the T-s plane, moving one temperature level and keeping in mind that the (1.4) has always to be fulfilled.

1.2 Real absorption chiller process

A real single stage absorption chiller retains the main characteristics of the ideal cycle described in 1.1. It is infact a device that provides a cooling effect Q_E, at the expense of a thermal input Q_G, rejecting a certain amount of heat Q_M. The transformations are though not reversible, and specifications on the real working fluids and on the chiller layout are necessary. For this purpose a diagram of a single stage LiBr – H_2O chiller is shown in Figure 1.3.

On the left hand side of Figure 1.3 two vessels can be individuated, a condenser (C) and an evaporator (E). These are also found in many other refrigerating machines (like vapor compression chillers). A refrigerant, that in the present case is pure water, is condensed in the high pressure vessel C, until it reaches the state of saturated liquid (point 8). The condensation process releases the latent heat Q_C to an external stream. The refrigerant is then brought to the low pressure vessel E through a lamination valve or a U tube (point 9). Due to the lamination it is now a mixture of vapor and liquid. In the evaporator the liquid part of the refrigerant is brought to the state of saturated vapor. The evaporation takes place thanks to a quantity of heat Q_E extracted from an external stream.

If water vapor (point 10) is taken again to the high pressure level the cycle can be closed. How this is accomplished is the key of the absorption technology.

The saturated vapor enters the vessel A, named absorber, which is at a pressure almost identical to that of the evaporator.

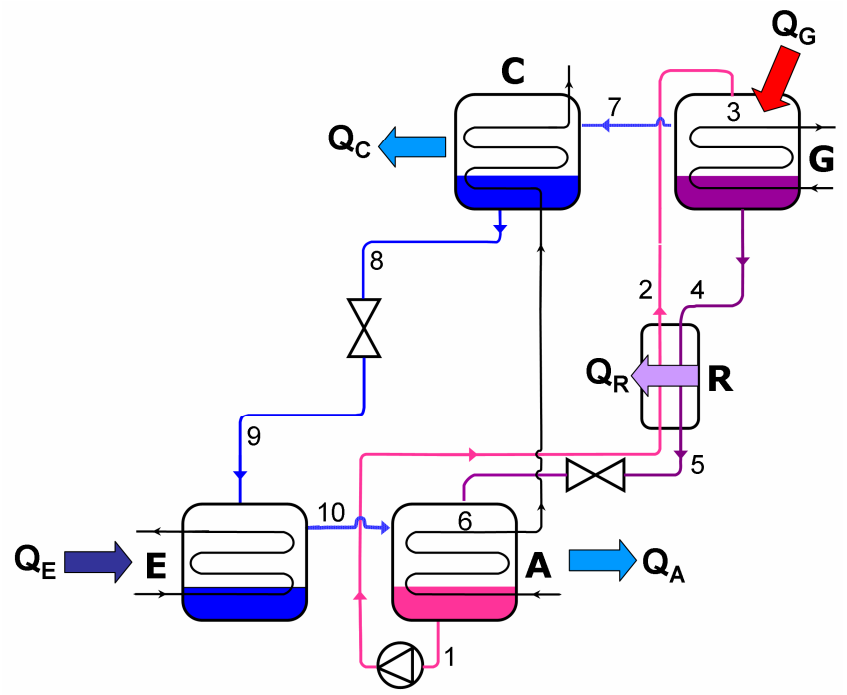

Figure 1.3 Schematic diagram of an absorption chiller

Here the refrigerant vapor is brought in contact with a strong solution of LiBr – H_2O (point 6), where strong means with a high concentration of LiBr. The water vapor begins to be absorbed into the strong solution, releasing both latent heat of condensation and heat of dilution Q_A. This heat is continuously drawn to an external stream, otherwise the absorption process would stop. At the bottom of the vessel the solution has a lower concentration of LiBr, due to the fact that the refrigerant is now within it in a liquid phase. This weak solution (point 1) is then pumped to the high pressure level, employing a very small quantity of mechanical work. The solution flows into a regenerative heat exchanger (R), where it receives a certain amount of heat Q_R (point 2). After the heat exchanger it enters the vessel G, named generator. In this vessel the weak solution is heated by a thermal input Q_G, taken from an external stream. The most volatile

component of the solution, which is the water, starts to evaporate and to leave the solution. The solution becomes strong again (point 4), while the refrigerant enters the condenser to begin the condensation (point 7). The strong solution (point 4), on its way back to the absorber, enters the regenerative heat exchanger R, where it is cooled down releasing a quantity of heat Q_R to the upcoming stream of the weak solution (point 5). Before entering the absorber it is brought to the low pressure level through a lamination valve or a U tube. Finally the strong solution enters the absorber (point 6).

2 Absorption chiller modeling

2.1 Background

As any application of the absorption chiller in a thermal system is considered, the need of predicting its performance with a certain degree of accuracy arises. Different absorption chiller models have been proposed in the literature, with different degree of detail. An important distinction is between steady state and transient modeling. Here only the former is considered.

Among the available models, one remarkable for its simplicity was developed by Hellmann et alii [Hellmann et al. 1998]. It describes the performance of an absorption chiller with only two algebraic equations, one for the chiller capacity and one for the COP. These equations can be easily solved, with little computational effort, and are well suited to be included in large simulation packages.

A more detailed model is the one of Grossman and Michelson [Grossman and Michelson 1985]. This model was included in a research software, ABSIM, developed at the Oak Ridge National Laboratory. The assumptions made in the ABSIM model are basically the same that will be employed in the following. More effort will be devoted in the present work to the off design operation of the heat exchangers dealing with the simulation of the Yazaki WFC10 chiller.

2.2 Structure of the model

Each component of the absorption chiller is modeled with a set of equations. These are energy balances for the internal and the external stream, and heat transfer rate equations.

A main mass balance is applied to the entire cycle, expressing the conservation of the refrigerant and of the salt. Other energy and mass balances are used to describe the lamination of the refrigerant, the lamination of the solution and the adiabatic absorption-desorption phenomenon. Each element is regarded as a module, as shown in Figure 2.1.

To complete the model, thermodynamics properties of the working fluids are needed. Two main property databases are provided, one for the pure

water, one for the LiBr-H_2O solution. Each module can invoke the property data to obtain fluid properties required in the balance equations.
All the equations resulting from the model have to be solved simultaneously. To perform this task the main program gives a unique name to the variables shared by the components and calls a system equation solver. The advantage of having a modular structure, instead of writing directly a system of equations, is that the modeling of any component can be improved in detail without affecting the main structure of the model.

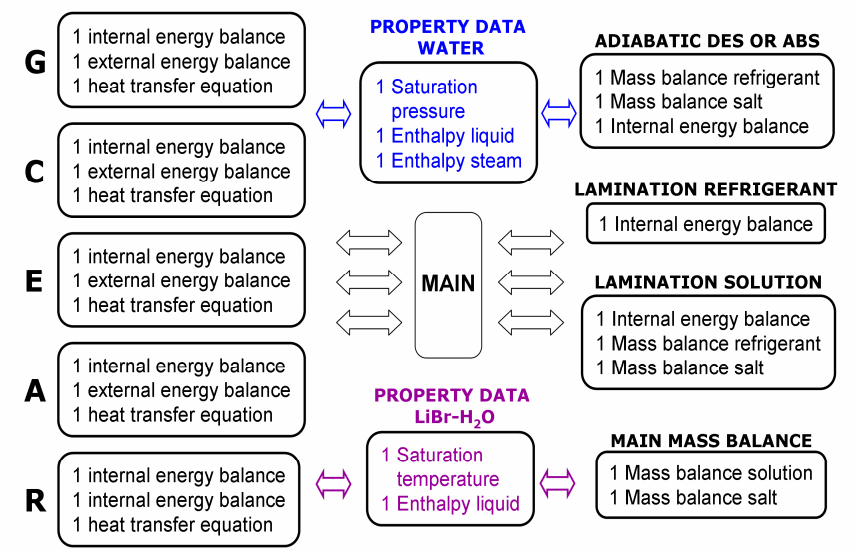

Figure 2.1 Structure of the computer absorption chiller model

2.3 Model assumptions

The following assumptions are made in the model:

1) Steady state conditions
2) The pressure in the condenser is equal to that of the generator; the pressure in the evaporator is equal to that of the absorber

3) Pressure changes occur only in the expansion valves and in the pump, there are no head losses along the tubes
4) No heat losses to the environment
5) Heat exchangers UA values do not depend on working conditions
6) Solution pump work is neglected both in COP calculation and in determination of weak solution properties
7) Weak solution flow rate is not dependent on the working conditions
8) The refrigerant leaves the condenser and the evaporator respectively as saturated liquid and saturated vapour
9) The weak solution leaving the absorber and the strong solution leaving the generator are assumed to be in saturated state
10) The superheated steam leaving the generator has a temperature equal to a mean between the weak solution entering the generator and the saturated strong solution leaving the generator

Assumption 1) is rarely verified during normal chiller operation. Nevertheless typical performance curves of absorption chillers are given as a set of working points under stationary conditions. So, for the purpose of a general modeling, such assumption can be justified. It remains to be discussed if this approach is then satisfactory when the model is included in a thermal system simulation. This depends mainly on the size of the chiller and on the type of system in which the chiller has to operate. If unsteady modeling might be desirable, it requires a good amount of information on the chiller construction, which is seldom available.

Assumption 2) is very well verified in most of the chillers. A typical design of the machine is in fact of the two shells type. Generator and condenser are built in an upper shell, while evaporator and absorber are built in a lower shell. The pressure in each shell is fairly constant everywhere.

Assumption 3) has a very small impact on model computation for two distinct reasons. First the number of points needed for the calculation is not so high along the tubes to require the exact value of pressure everywhere. Second the pressure has little effect on the enthalpy of the liquid solution, so it has small influence on the energy balances.

Assumption 4) is not verified in real machines. The amount of losses changes very much from chiller to chiller, depending on how they are insulated. Generator and evaporator are most likely to loss and gain heat

respectively, but depending on environment temperature gain or losses from condenser and absorber are also possible. These losses can have a variable effect on the chiller performance; in the model they are not taken into account because they are too specific for each chiller and they would add useless complexity to the overall energy balance.
Assumption 5) is quite critical. The heat transfer characteristics of chiller components can vary considerably during operation. As the absorption machine is made essentially of five heat exchangers, this has a remarkable effect on the performance. Not every chiller has the same behavior under this respect. The main goal of a chiller manufacturer is actually to obtain a machine with good heat transfer characteristics under part load conditions, otherwise both the capacity and the efficiency can rapidly deteriorate. In the present work this assumption will be removed in the simulation of the Yazaki WFC-10, as it would lead to unrealistic results in the prediction of the off-design operation. For other chillers it can be employed, allowing an acceptable modeling.
Assumption 6) is very frequently employed in absorption chiller analysis. The mechanical work input is negligible in comparison with the thermal energies exchanged at the generator and at the evaporator. For their small entity the effects of the pump work on the weak solution properties can be neglected.
Assumption 7) is again dependent on the type of chiller considered. For mechanical solution pump, like the one in Figure 2.1, the external characteristic of the circuit has small changes during operation. For heat driven pump, like the one employed in the Yazaki WFC 10, this flow can vary considerably.
Assumption 8) is usually satisfied in absorption chillers. Subcooling of the refrigerant leaving the condenser is also possible, but the amount is not significant and there are small experimental evidences of it.
Assumption 9), like assumption 5), can be unrealistic under certain operating conditions. In both the generator and the absorber a physical process takes place that includes heat and mass transfer. Taking the absorber as example, the most desirable case is that the heat exchanged is employed uniquely to reject the heat of condensation and dilution of the vapor absorbed into the solution. The result in this case would be to have at the absorber outlet a saturated weak solution. But if after the overall process the exiting solution has a certain degree of subcooling, this means

that the heat rejection is not employed effectively. In fact the weak solution needs to be heated in the generator, to separate the refrigerant from it, and any subcooling at the absorber outlet requires additional heat input at the generator.
A similar argument can be made on the solution state at the generator outlet. If it is superheated the heat input is not employed in the most efficient way. As a matter of fact the solution state at the outlet of these two components gives an important indication on the chiller performance. The presence of subcooling and superheating can change significantly the capacity and the COP of a chiller. Experimental and theoretical evidence of subcooling at the absorber outlet has been reported in literature. More recently also experimental detection of superheating at the generator outlet has been claimed [Enke 2007].
Assumption 10) is verified depending on the arrangement of the generator heat exchanger. The temperature of the leaving vapor is between the temperature of the entering weak solution and the exiting strong solution. In the case of a falling film generator, where the solution falls from the top of the generator, while the heating fluid flows from the bottom to the top of the tube bundle, the leaving temperature of the vapor is likely to be a mean of the solution temperatures. Since the quantity of vapor released is not even through the tube bundle, the resulting temperature can be closer to one of the boundary values. The effect on computation is in any case not relevant.

2.4 Model equations

The equations employed in the model are here reported following the modular structure of Figure 2.1 and the points numbering of Figure 1.3. Temperatures of the internal streams are written in capital letters to distinguish them from temperatures of the external streams.

2.4.1 Generator

One internal and one external energy balance:

$$Q_G + m_w h_{Rwo} - m_r h_{Ci} - m_s h_{Rsi} = 0 \tag{2.1}$$

$$Q_G - m_G \left(h_{Gi} - h_{Go} \right) = 0 \tag{2.2}$$

One heat transfer rate equation:

$$Q_G = UA_G \Delta T_{lmG} \tag{2.3}$$

$$\Delta T_{lmG} = \frac{\left(T_{Go} - t_{w3}\right) - \left(T_{Gi} - t_{Rsi}\right)}{\ln \frac{\left(T_{Go} - t_{w3}\right)}{\left(T_{Gi} - t_{Rsi}\right)}} \tag{2.4}$$

2.4.2 Condenser

One internal and one external energy balance:

$$Q_C - m_r \left(h_{Ci} - h_{Co}\right) = 0 \tag{2.5}$$

$$Q_C - m_{AC} \left(h_{ACo} - h_{exCi}\right) = 0 \tag{2.6}$$

One heat transfer rate equation:

$$Q_C = UA_C \Delta T_{lmC} \tag{2.7}$$

$$\Delta T_{lmC} = \frac{\left(t_{Ci} - t_{ACo}\right)}{\ln \frac{\left(T_C - t_{ACo}\right)}{\left(T_C - t_{exCi}\right)}} \tag{2.8}$$

2.4.3 Evaporator

One internal and one external energy balance:

$$Q_E - m_r \left(h_{Eo} - h_{Ei}\right) = 0 \tag{2.9}$$

$$Q_E - m_E \left(h_{exEo} - h_{exEi}\right) = 0 \tag{2.10}$$

One heat transfer rate equation:

$$Q_E = UA_E \Delta T_{lmE} \tag{2.11}$$

$$\Delta T_{lmE} = \frac{\left(t_{Eo} - t_{Ei}\right)}{\ln \frac{\left(t_{Eo} - T_E\right)}{\left(t_{Ei} - T_E\right)}} \tag{2.12}$$

2.4.4 Absorber

One internal and one external energy balance:

$$Q_A + m_w h_{Rwi} - m_r h_{Eo} - m_s h_{Rso} = 0 \tag{2.13}$$

$$Q_A - m_{AC}\left(h_{exCi} - h_{ACi}\right) = 0 \tag{2.14}$$

One heat transfer rate equation:

$$Q_A = UA_A \Delta T_{lmA} \tag{2.15}$$

$$\Delta T_{lmA} = \frac{\left(T_{Rwi} - t_{ACi}\right) - \left(T_{Rso} - t_{Ci}\right)}{\ln \frac{\left(T_{Rwi} - t_{ACi}\right)}{\left(T_{Rso} - t_{Ci}\right)}} \tag{2.16}$$

2.4.5 Regenerative heat exchanger

Two internal energy balances, one for the weak solution and one for the strong solution:

$$Q_R - m_w\left(h_{Rwo} - h_{Rwi}\right) = 0 \tag{2.17}$$

$$Q_R - m_s\left(h_{Rsi} - h_{Rso}\right) = 0 \tag{2.18}$$

One heat transfer rate equation:

$$Q_R = UA_R \Delta T_{lmR} \tag{2.19}$$

$$\Delta T_{lmR} = \frac{\left(T_{Rso} - T_{Rwi}\right) - \left(T_{Rsi} - T_{Rwo}\right)}{\ln \frac{\left(T_{Rso} - T_{Rwi}\right)}{\left(T_{Rsi} - T_{Rwo}\right)}} \tag{2.20}$$

2.4.6 Adiabatic desorption or absorption

As the solution enters the generator it is rarely in a saturated state. Depending on the performance of the regenerative heat exchanger it can be either superheated or subcooled. After entering the distributor two situations might arise. If the solution is superheated, water vapour flashes in the generator chamber. This is called adiabatic desorption, as the vapour is desorbed from the solution without adding heat to it. If the solution is subcooled, it has the ability to absorb some water vapour before actually getting in contact with the heat exchanger tube bundle. This second case is called adiabatic absorption, as the vapour is absorbed into the solution without cooling it down. In the adiabatic absorption the solution reaches the equilibrium state if it has enough contact time with the vapour. In the model it is supposed that the design of the chiller is such that the solution has time to reach an equilibrium condition. Strictly speaking the phenomenon here described has no influence on the energy balance (2.1), which considers a control volume that surrounds the whole generator. It has though an influence on the temperature of the solution as it begins to exchange heat with the external stream, therefore on the $\Delta T_{lm\,G}$.
The equations for the adiabatic desorption are two mass balances, one for the solution and one for the salt:

$$m_{r3} + m_{w3} - m_w = 0 \tag{2.21}$$

$$m_w x_w - m_{w3} x_{w3} = 0 \tag{2.22}$$

And one internal energy balance:

$$m_w h_{Rwo} - m_{r3} h_{Ci} - m_{w3} h_{w3} = 0 \tag{2.23}$$

In the case of adiabatic absorption the refrigerant mass balance becomes:

$$m_{r3} + m_w - m_{w3} = 0 \tag{2.24}$$

The internal energy balance is:

$$m_w h_{Rwo} + m_{r3} h_{Ci} - m_{w3} h_{w3} = 0 \tag{2.25}$$

2.4.7 Lamination refrigerant

The lamination of the refrigerant is considered isoenthalpic and can be described by the energy balance:

$$m_r (h_{Co} - h_{Ei}) = 0 \tag{2.26}$$

2.4.8 Lamination solution

The lamination of the solution is considered to be isoenthalpic. The average composition of the flow does not change during the process, but after a pressure drop the solution may be in the state of a vapor-liquid mixture. The equations to describe the lamination are one energy balance:

$$m_w h_{Rso} - m_{r6} h_{r6} - m_{w6} h_{w6} = 0 \tag{2.27}$$

Two mass balances, one for the solution and one for the salt:

$$m_{r6} + m_{w6} - m_w = 0 \tag{2.28}$$

$$m_w x_w - m_{w6} x_{w6} = 0 \tag{2.29}$$

2.4.9 Main mass balance

An overall mass balance can be applied to the internal streams of the chiller. It is made of two equations, one mass balance for the solution and one for the salt:

$$m_s + m_r - m_w = 0 \tag{2.30}$$

$$m_w x_w - m_s x_s = 0 \tag{2.31}$$

2.4.10 Property data water

Thermodynamics properties of the refrigerant are needed in the model to employ the equations described so far. The most up to date correlations on water properties have been published by Wagner et al. [Wagner et al. 2000]. They are expressly made to ensure both accuracy and computational efficiency. Considering the main states in which water is found throughout an absorption chiller, the following three relations are necessary. The enthalpy of liquid water as a function of the temperature and pressure:

$$\begin{aligned} & h_{liq} = f(T, p) \\ & 273.15 <= T <= 623.15 \text{ K} \\ & p_{sat}(T) < p < 100 \text{ MPa} \end{aligned} \tag{2.32}$$

The enthalpy of steam as a function of the temperature and pressure:

$$\begin{aligned} & h_{steam} = f(T, p) \\ & 273.15 <= T <= 623.15 \text{ K} \\ & 0 < p <= p_{sat}(T) \end{aligned} \tag{2.33}$$

The saturation pressure on the vapor-liquid saturation curve as a function of temperature:

$$\begin{aligned} & p = p_{sat}(T) \\ & 273.15 <= T <= 647.096 \text{ K} \end{aligned} \tag{2.34}$$

2.4.11 Property data LiBr-water solution

As for the refrigerant some thermodynamics properties of the LiBr-water solution complete the equations of the model. The existence of reliable correlations is in this case less established in the literature. Most of the works report on limited set of data and to cover wide range of concentrations the usage of more than one equation might be necessary. An attempt to face this kind of problem has been made by Hellmann and Grossman [Hellmann and Grossman 1996]. They review and select recent correlations, with the aim of making them suitable for computer

simulations. Based on their publication the following relations are employed. Boiling temperature of the solution as a function of the concentration and of the saturation water temperature corresponding to the desired pressure:

$$\begin{aligned} &T = f\left(x, T_{sat,r}\left(p\right)\right) \\ &273.15 \le T_{sat,r} \le 463.15\,\mathrm{K} \\ &0 \le x \le 76\% \end{aligned} \tag{2.35}$$

Enthalpy of the solution as a function of the temperature and concentration:

$$\begin{aligned} &h = f\left(T, x\right) \\ &273.15 \le T \le 435.15\,\mathrm{K} \\ &0 \le x \le 70\% \end{aligned} \tag{2.36}$$

2.5 Solver requirements

The entire set of model equations forms a non linear system. The heat transfer rate formulation and especially the property data functions contain highly non linear terms. From a mathematical point of view this kind of system can have more than one solution. Care must be taken to assure that the final solution has physical meaning.

A survey on the standard algorithms implemented by commercial software has shown that both Matlab [MathWorks 2002] and EES [Klein et al. 1990] can be employed to solve the present problem. The latter has the noteworthy advantage that the user can define a domain of existence for the solution. This is done thanks to a series of linear inequalities applied to the variables. Moreover, defining some dummy variables, linear relations between different temperatures and other quantities can be implemented. Typical constraints on the solution are for instance: decreasing temperatures in the direction of heat transfer, weak solution concentration smaller than the strong one, condenser pressure higher than evaporator pressure.

3 Modeling of the Thermax chiller

3.1 Model input

The model described in chapter 2 is here employed to predict the performance of a commercial chiller. The equations presented so far can be solved if a certain number of variables are given as input. A quite natural choice is to choose a number of variables which depend on the chiller construction. These are the product of the overall heat transfer coefficient U and the heat exchange area A for each component, and the mass flow rate of the weak solution m_w. If a mechanical pump is employed, this flow rate is determined by the intersection of the pump characteristic with the characteristic of the circuit.
As the chiller is part of a thermal system or of a system simulation program, other variables are usually known. These are the mass flow rates and the inlet temperatures of the external streams. Neglecting the external influence of the environment temperature, a given set of these variables determines the chiller performance. In fact, the typical experimental characterization of an absorption chiller includes a series of tests where the flow rates of the external streams are fixed and the inlet temperatures are changed in gradual steps. As steady state conditions are reached, each combination of these temperatures individuates a specific working condition.
Unfortunately the design characteristics of a chiller are seldom available from a manufacturer. So, unless a dedicated test rig is constructed, both the UA values of the heat exchangers and the weak solution flow rate m_w have to be determined numerically.
To do so the knowledge of the nominal working conditions of a chiller can be exploited. This kind of data is typically available for commercial chiller and it reduces the number of unknowns of the set of equations. To close the problem still one variable has to be assumed; the evaporation temperature can be reasonably guessed for instance.

3.2 Modeling of the Thermax chiller: results

The model has been applied to predict the off design performance of the Thermax LT-42 chiller. The nominal working conditions of this chiller,

according to the manufacturer, are reported in Table 3.1. Assuming an evaporation temperature T_E equal to 5 °C the UA values shown in Table 3.2 are calculated. The weak solution mass flow rate is equal to 12 kg/s.
To present the performance curves of the chiller, one of the following three temperatures of the external streams is varied, keeping the other two at their nominal values: the inlet temperature at the generator (t_{Gi}), the inlet temperature at the condenser (t_{CAi}) and the outlet temperature at the evaporator (t_{Eo}). The effect on the chiller capacity and on the COP of this individual change is calculated.

Nominal working conditions of Thermax LT-42			
Q_E = 1471 kW	Q_G = 1978 kW	$Q_A + Q_C$ = 3449 kW	
Chilled water	m_E = 70 kg/s	t_{Ei} = 12 °C	t_{Eo} = 7 °C
Cooling water	m_{AC} = 147 kg/s	t_{ACi} = 29 °C	t_{ACo} = 34.6 °C
Hot water	m_G = 47 kg/s	t_{Gi} = 90 °C	t_{Go} = 80 °C

Table 3.1 Nominal operating conditions of the Thermax LT-42 declared by the manufacturer

UA_G	UA_C	UA_E	UA_A	UA_R
218 kW/K	203 kW/K	368 kW/K	360 kW/K	64 kW/K

Table 3.2 Calculated UA values for the Thermax LT-42 chiller

The LT-42 has the characteristic that condenser and absorber are cooled in series, with the condenser being the first element. A more common configuration, which has been considered writing the equations of chapter 2.4, is the one with the absorber as the first cooled component.
The results are compared to the off-design curves available from the manufacturer, showing in general a good agreement between the model and the declared data.

3.2.1 Effects of the inlet hot temperature at the generator

In Figure 3.1 are reported the effects on the chiller capacity of a variation of the inlet hot temperature at the generator (t_{Gi}) from 75 to 103 °C. The other two temperatures of the external streams are kept at their nominal values (t_{ACi}=29 °C, t_{Eo}=7 °C). The capacity increases as the inlet temperature at the generator increases. The maximum relative error between the model and the manufacturer data is 6 %, it occurs at t_{Gi}=75 °C. The effects of the hot inlet temperature on the COP are shown in Figure 3.2.

No data are available from the manufacturer in this case. So, a part from the nominal COP, a comparison between predicted performance curve and data is not possible. The chiller COP rises with the hot water temperature. The gain in efficiency is not so remarkable from temperatures higher than 90 °C. For very high temperatures the COP levels off and it even slightly decreases.

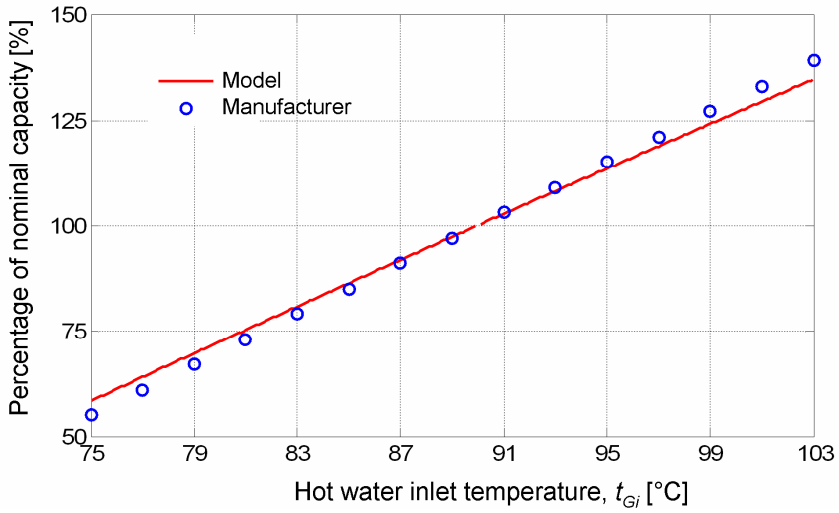

Figure 3.1 Effects of the hot water inlet temperature on the Thermax chiller capacity

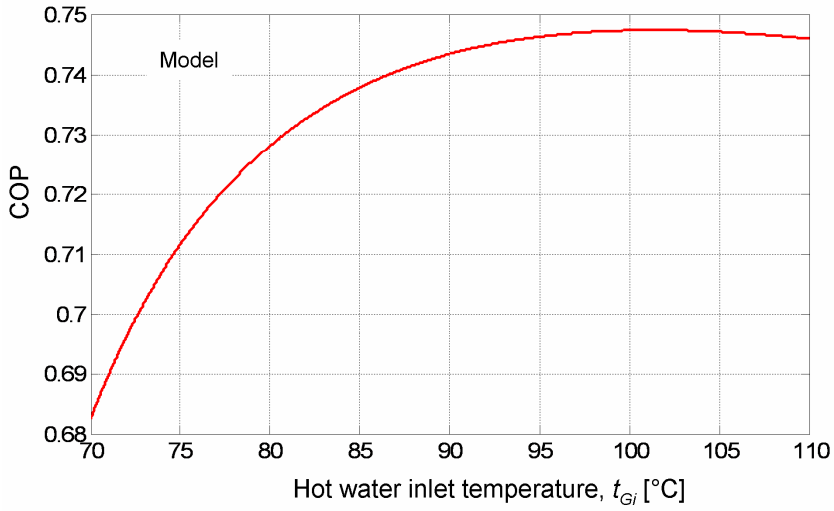

Figure 3.2 Effects of the hot water inlet temperature on the Thermax chiller COP

Temperatures in the range from 70 to 90 °C can be obtained with many solar collectors available on the market, starting from well insulated flat plate collectors to evacuated tube collectors.

3.2.2 Effects of the chilled water outlet temperature at the evaporator

In Figure 3.3 are reported the effects on the chiller capacity of a variation of the chilled water outlet temperature (t_{Eo}) from 5 to 10 °C. The other two temperatures of the external streams are kept at their nominal values (t_{ACi}=29 °C, t_{Gi}=90 °C).

The capacity of the chiller increases with increasing temperatures of the chilled water. The comparison with the manufacturer data shows a maximum relative error of 3% for a temperature t_{Eo} equal to 10 °C.

The COP curve shown in Figure 3.4 is very similar, with the COP rising with rising t_{Eo} temperature. No data are available from the manufacturer in this case.
As the chiller is employed to cool a building some considerations can be drawn on the temperature of the chilled water. As seen from the curves, a higher temperature of the chilled water results in higher capacity and COP. But if the cooling load of the building has a significant portion of latent demand, a high chilled water temperature might be not suitable to perform dehumidification.

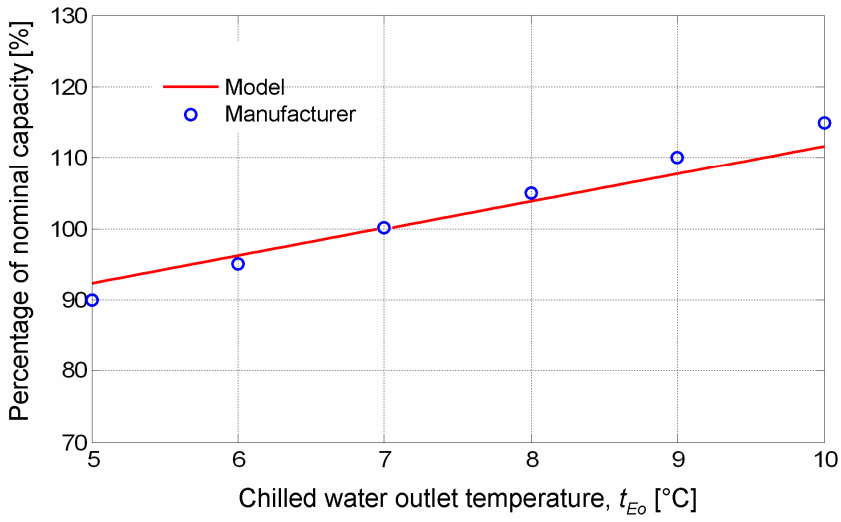

Figure 3.3 Effects of the chilled water outlet temperature on the Thermax chiller capacity

For this reason, attention should be paid on the type of load to be satisfied. In cases where humidity is not a big issue, radiant cooling can be employed, with higher chilled water temperatures and better performance of the chiller.

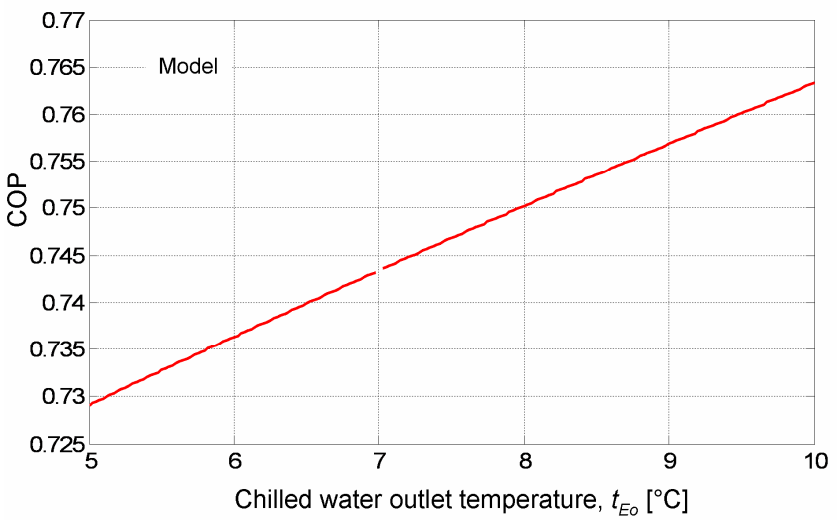

Figure 3.4 Effects of the chilled water outlet temperature on the Thermax chiller COP

3.2.3 Effects of the cooling inlet temperature at the condenser

In Figure 3.5 are reported the effects on the chiller capacity of a variation of the cooling inlet temperature at the condenser (t_{CAi}) from 20 to 34 °C. The other two temperatures of the external streams are kept at their nominal values (t_{Eo}=7 °C, t_{Gi}=90 °C).

The data calculated from the model agree to a certain extent with the data declared by the manufacturer. The maximum relative error of the calculation is of 11.6 % for a temperature t_{CAi} equal to 34 °C. It is evident though that the manufacturer curve has a shape which is not entirely reproduced by the modeling. The two assumption 5) and 9), stated in chapter 2.3, might be oversimplifying in this case. But the knowledge of the chiller, based on the declared manufacturer data, is not deep enough to make other reasonable hypotheses.

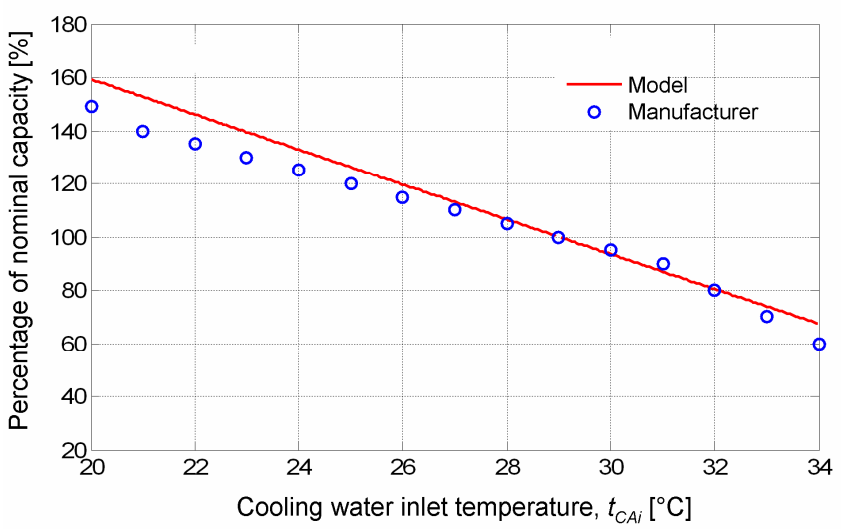

Figure 3.5 Effects of the cooling water inlet temperature on the Thermax chiller capacity

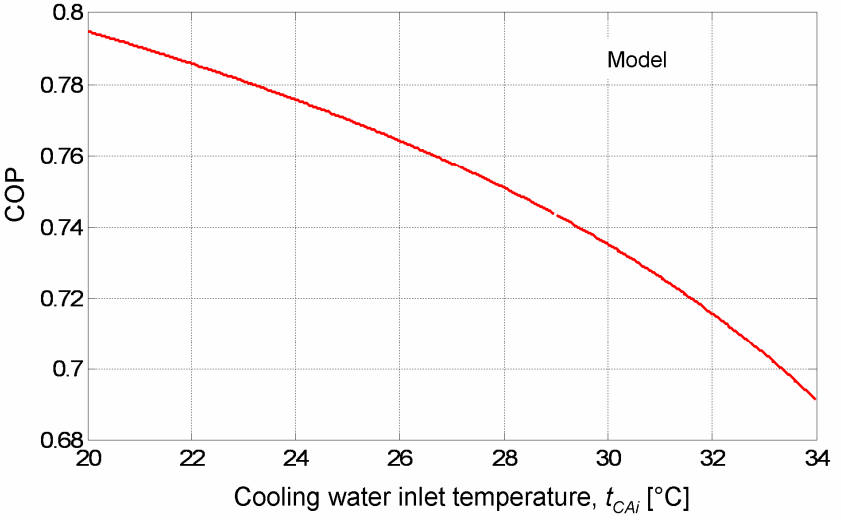

Figure 3.6 Effects of the cooling water inlet temperature on the Thermax chiller COP

The effects on the COP of the cooling water inlet are reported in Figure 3.6. No off design data on the COP are available from the manufacturer.
As the plots show, the cooling water temperature has a strong influence on the performance of the chiller. Both capacity and COP increase for decreasing cooling temperature.
A common technology employed for the heat rejection of an absorption chiller is a wet cooling tower. This type of cooling garantees lower inlet temperatures than dry cooling, but at the expense of higher capital and running costs. Balance between energy performance of the chiller and cost of the heat rejection has to be consided carefully. Furthermore high cooling temperatures can lead to crystallization of the strong solution if the other two external temperatures are not properly controlled.

4 Modeling of the Yazaki WFC-10 chiller

4.1 Principal caracteristics of the WFC-10

The WFC-10 is a 35 kW absorption chiller produced by the japanese company Yazaki.
It has the distinct characteristic of employing a heat driven pump on the solution circuit. This kind of pump, named bubble pump from its working principle, is integrated in the generator of the machine. The thermal input delivered to the generator has the combined effect of evaporating the refrigerant and promoting the solution circulation.
Unlike most of the absorption chillers the WFC-10 has no refrigerant circulation pump. This pump is usually used to ensure a good wetting of the evaporator tube bundle. So, the chiller on its own has no mechanical pumps. This means that no electrical energy input is necessary to drive the internal flows.
The performance of the WFC-10 is analysed here using an evolution of the model described in chapter 2 and the experimental data retrieved by a test rig installed in the Press and Information Office of Berlin (BPA).

4.2 Performance curves

The performance curves of the WFC-10 are given by the manufacturer for fixed couples of the hot and cooling water inlet temperatures, varying the chilled water outlet temperature. Unlike the curves presented in chapter 3 for the Thermax chiller, the effects of a continuos variation of an external temperature are reported only for the chilled water outlet temperature.
Figure 4.1Figure 4.1 and Figure 4.2 show the capacity and the COP of the chiller varying the chilled water outlet temperature. Continuos line is used for the manufacturer data while circles are used for the experimental data. It can be noted that there is a certain deviation between the curves. The measured capacity is lower than the one declared by the manufacturer. A reason for this deviation can be the particular heat carrier fluid used in the external circuit at the generator (in the test rig it is a mixture of water and glycole propilene), which lowers the heat transfer coefficient of the heat exchanger.

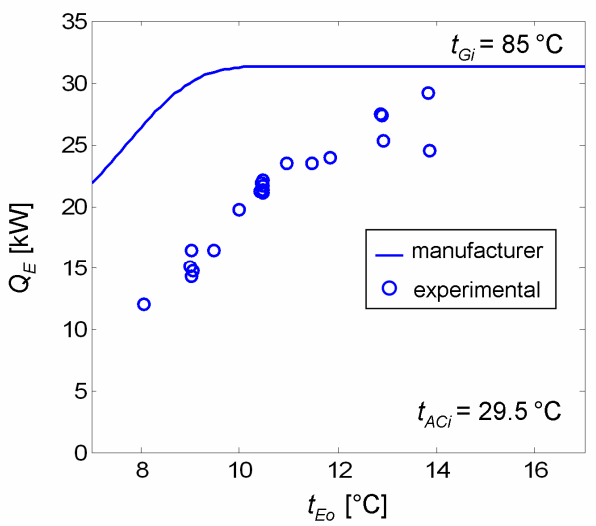

Figure 4.1 Effects of the chilled water outlet temperature on the WFC-10 capacity

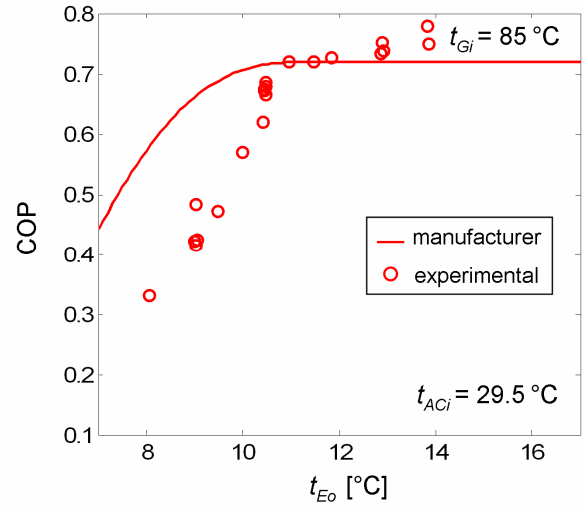

Figure 4.2 Effects of the chilled water outlet temperature on the WFC-10 COP

The behaviour of the chiller appears clearly from the curves: both the capacity and the COP drop for low chilled water temperature, whereas they level off for high chilled water temperature.

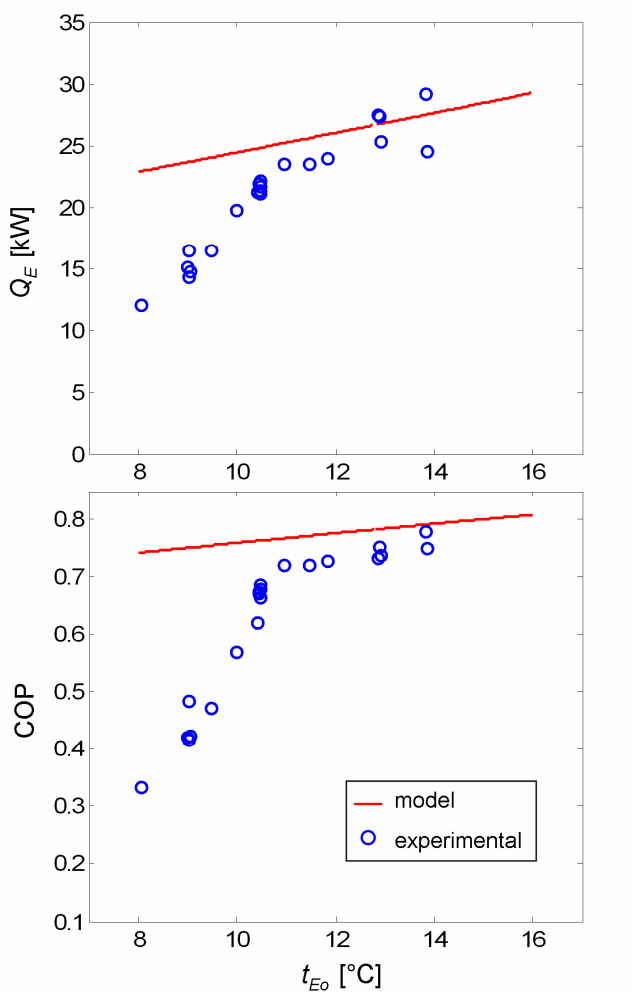

Figure 4.3 Performance of the WFC-10 chiller: comparison between basic model and experimental data

There is a remarkable difference between the way the WFC-10 and the Thermax chiller performs. As shown in Figure 3.3 the capacity of the Thermax chiller does not decrease so steeply as the chilled water temperature is decreased. Moreover the capacity tends to increase with high chilled water temperature instead of becoming constant.
Other chillers, like the SonnenKlima [Petersen et al. 2006], behave like the Thermax, showing that the WFC-10 is a case on its own.
As it could be expected, the model described so far gives a non satisfactory result if applied to the WFC-10. This is shown in Figure 4.3.

4.3 Measuring instrumentation

The experimental set up of the WFC-10 is located in the Press and Information Office (BPA) in Berlin. The chiller has been monitored for research purpose by the Technische Universität Berlin, Institut für Energietechnik.
The main sensors employed to analyse the chiller are shown in Figure 4.4

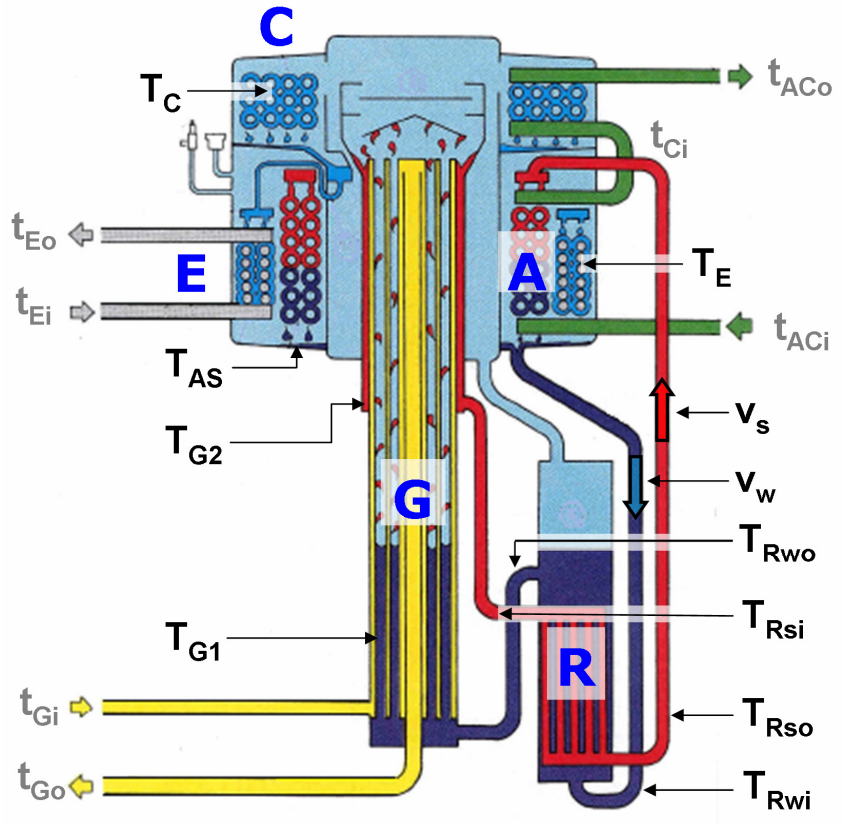

Figure 4.4 Scheme of the WFC-10 measuring instrumentation

All the temperatures are measured with calibrated Pt-100 resistance thermometers, the flow velocity of the weak (v_w) and of the strong (v_s)

solution is measured with ultrasonic sensors of type FLUXUS ADM 6402. Other sensors not shown in Figure 4.4 include magnetic inductive flow meters for the external streams, together with heat meter of type CALEC MB. These provide a measure of the thermal power exchanged by the chiller.

4.4 Experimental analysis

The background to the experimental analysis presented here are two papers from Albers et alii [Albers 2003, Albers 2005]. Some of the results of these works will be illustrated as they serve to the general understanding of the WFC-10 chiller and its consequent modeling.

The flow velocity measurements could be exploited to calculate the internal mass flow rates of the chiller, i.e. the weak solution flow rate m_w and the strong solution flow rate m_s. The refrigerant flow rate $m_{r,tot}$ might be obtained then from equation (2.30).

Nevertheless, the extremely unsteady nature of the bubble pump causes the velocity measurement to be quite uncertain. Especially the strong solution flow velocity oscillates widely, assuming values close to zero that are not accurately detected by the ultrasonic sensor.

A more convenient choice is to assume, within its uncertainty, the flow velocity of the weak solution as a trusted value. The weak solution mass flow is calculated knowing the density of the solution and the tube geometry. A typical result of this step is shown in Figure 4.5. Then, using energy and mass balances, the strong solution flow rate as well as the refrigerant flow rate can be calculated from other measured variables.

As the present analysis is concerned with the steady state characterization of the chiller, before proceeding to all the mass flows calculation, the measurements are averaged over periods of 20 minutes.

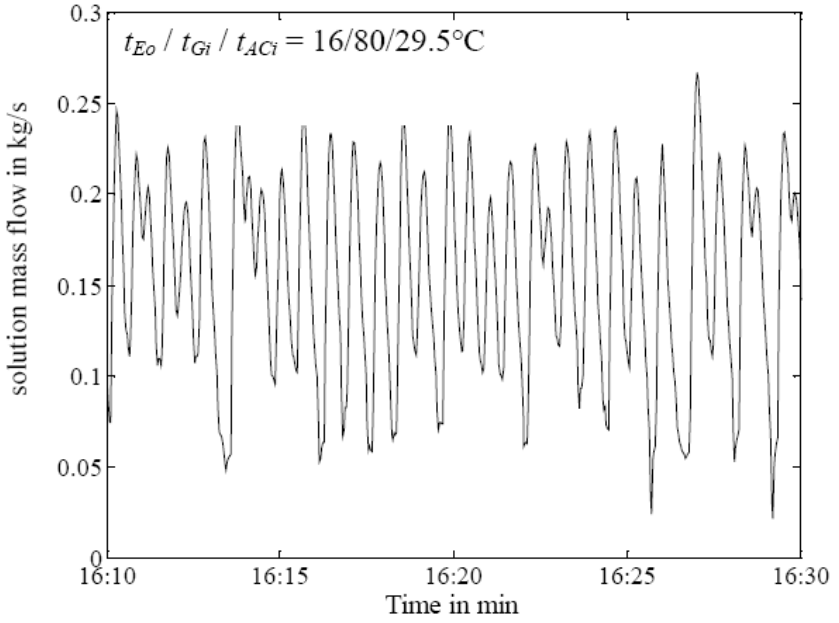

Figure 4.5 Weak solution flow rate in the Yazaki WFC-10 (from Albers et al. 2003).

The refrigerant flow rate and the weak solution flow rate are reported in Figure 4.6 together with the capacity curve of the chiller. It can be seen that the refrigerant flow rate, as well as the weak solution flow rate, doesn't change significantly along the entire performance curve.
If it is assumed that the capacity of a chiller is directly proportional to the quantity of refrigerant evaporated in the evaporator, it follows that not all $m_{r,tot}$ is being evaporated through the curve.
Following the schematization proposed by Albers and Ziegler [Albers and Ziegler 2003], three different domains can be individuated. In domain 1 the refrigerant desorbed in the generator is only partially evaporated in the evaporator. In domain 2 the refrigerant desorbed in the generator is almost entirely evaporated in the evaporator, the chiller achieves a good COP.
In domain 3 the refrigerant desorbed in the generator is evaporated in the evaporator, but although the chilled water temperature is increased no change in the capacity nor in the COP is observed.

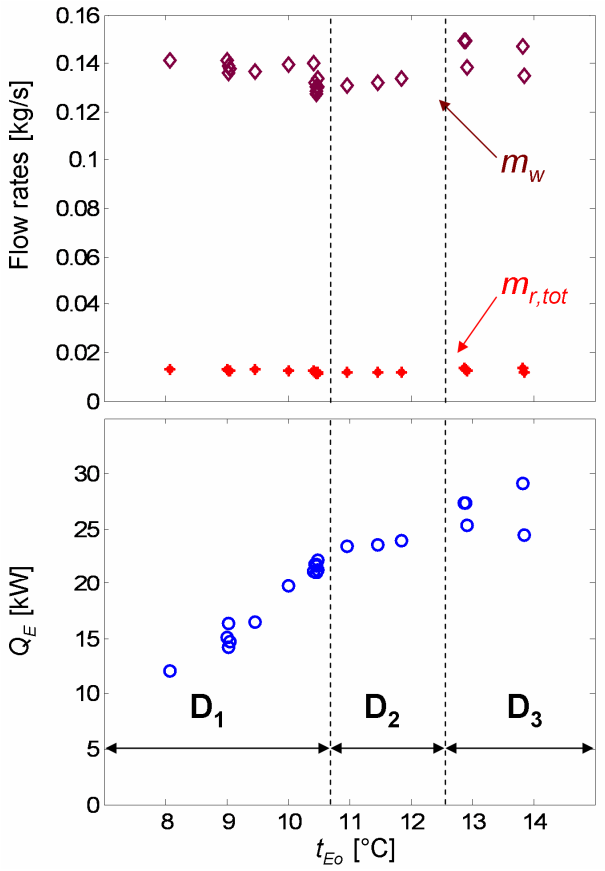

Figure 4.6 Refrigerant and weak solution flow rate along the perfomance curve of the WFC-10

Basically in domain 2 the chiller performs like a common absorption chiller with mechanical pumps. In the remaining domains two important phenomena take place.
In domain 1 the refrigerant which is not evaporated flows in the absorber sump. A careful look at Figure 4.4 reveals that evaporator and absorber share the same compartment. Since there is no refrigerant circulation pump the only technical solution to get rid of liquid refrigerant is its

mixing with the weak solution coming from the absorber. The solution flows then to the regenerative heat exchanger.

In domain 3 no liquid refrigerant goes into the absorber sump. The evaporator heat exchanger has here a very specific behaviour. Figure 4.7 shows the external temperatures at the evaporator, t_{Eo} and t_{Ei}, and the internal evaporation temperature T_E. In domain 3 the driving potential for the heat exchange process rises with rising chilled water temperature t_{Eo}.

As the capacity is fairly constant in this domain, it means that the characteristics of the heat exchanger are deteriorating. The increase in the temperature driving potential intensifies the refrigerant evaporation on the first rows of the tube bundle.

As shown schematically in Figure 4.8 the lower rows of the heat exchanger are wetted by a decreasing amount of liquid. Therefore for increasing chilled water outlet temperature the evaporator area effectively employed decreases.

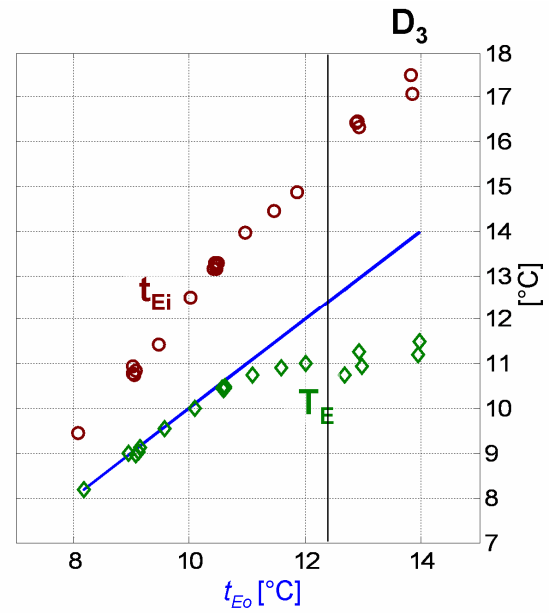

Figure 4.7 Increasing driving potential for heat transfer in the domain 3 of the performance curve

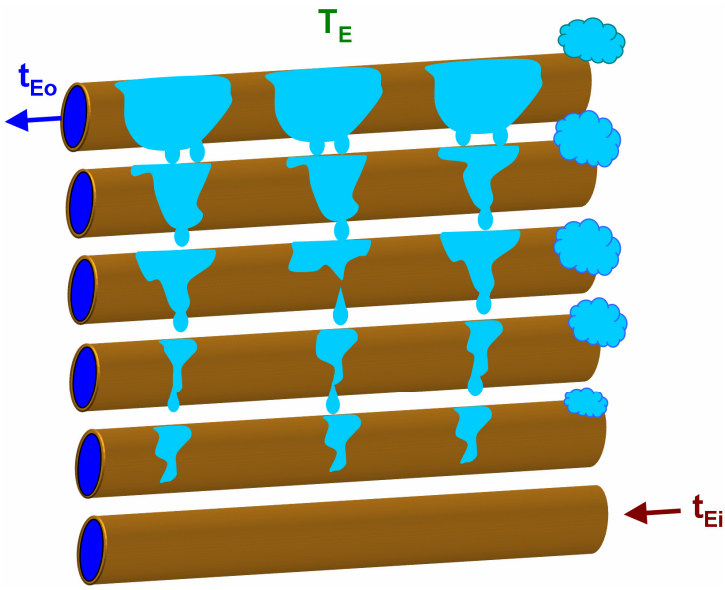

Figure 4.8 Schematic diagram of the evaporator tube bundle with dry areas

4.5 Internal flows as a function of the temperature thrust

As mentioned in chapter 4.4 the internal flows of the WFC-10 can be computed from the experimental data. A sistemathic study of the flows has been conducted in Albers et alii [Albers et al. 2005], to analyse the behaviour of the bubble pump.

Result like the one reported in Figure 4.6 shows that the internal flows are not very affected by a change in the chilled water temperature. It remains to be seen if the other two external temperatures, namely the inlet temperature at the generator t_{Gi} and the inlet temperature at the absorber t_{ACi} , have an effect on the internal flows.

A convenient way is to correlate the flows with the external temperature thrust, t_{Gi} - t_{ACi}. This is shown in Figure 4.9.

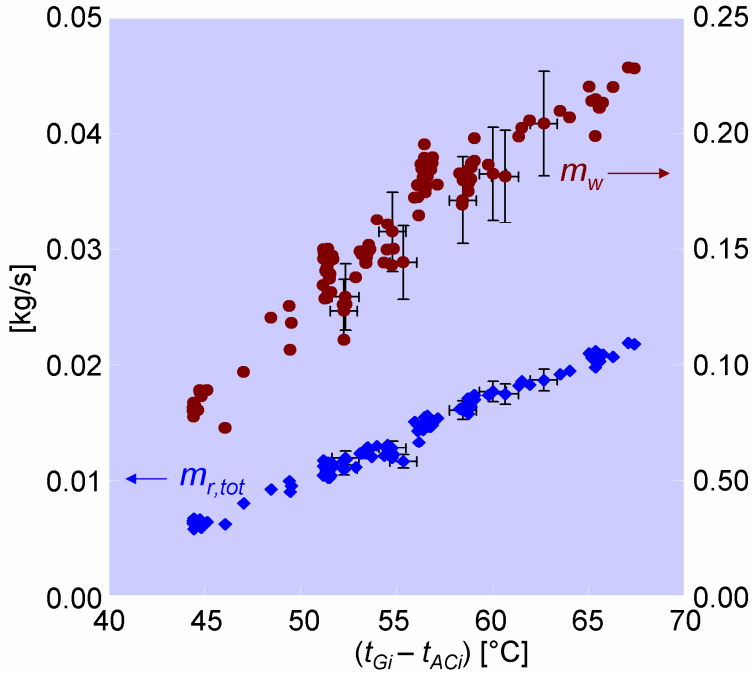

Figure 4.9 Dependence of the internal flow rates on the temperature thrust ($t_{Gi} - t_{ACi}$). From Albers et al. 2005.

There is a dependence of the refrigerant flow rate on the temperature thrust and it can be assumed in a first approximation to be linear. A similar dependence appears also for the weak solution flow rate, although the scatter of the data is more pronounced.
The correlation between the internal flows and the temperature thrust will be employed in the modeling of the WFC-10.

4.6 Heat exchangers characterization

The evaporator behaviour in domain 3 suggests that the approach described so far, of assuming constant *UA* values in absorption chiller modeling, does not apply to the WFC-10. Moreover, the internal temperature sensors give the opportunity to analyse the heat exchangers performance with some detail.

The analysis of the heat exchangers will be organised following the rappresentation of the performance curves. The aim will be to assess what type of variation, if present, occurs in the performance of the heat exchangers along different performance curves.
The degree of detail used in the analysis, as well as the consequent modeling, depends on the information available on the heat exchanger geometry and on the complexity of the heat transfer process.

4.6.1 Generator heat exchanger

The thermosyphon generator is a key element of the WFC-10. Here both the desorption process and the bubble pump action take place. The performance of the exchanger is reported in terms of the overall UA value.

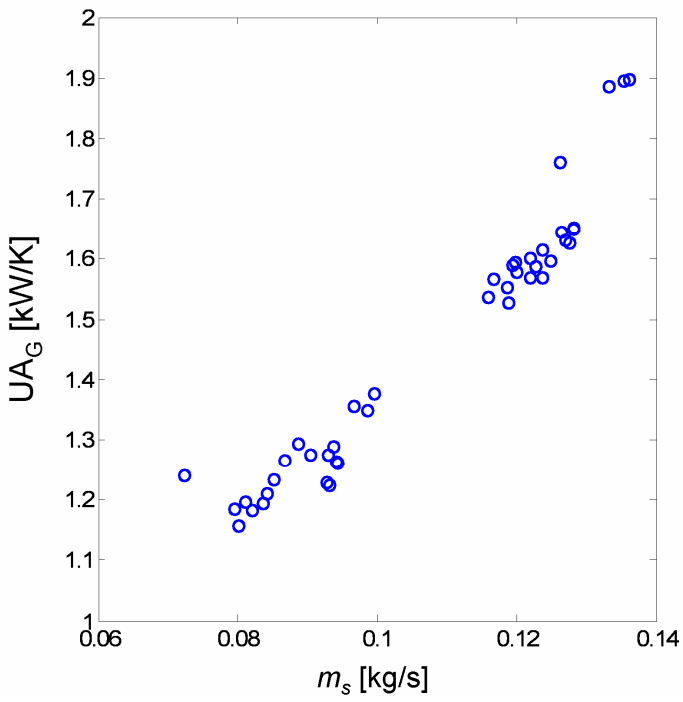

Figure 4.10 Variation of the generator UA value with the strong solution flow rate

This has a dependence on the external temperature thrust, i.e. it changes from a performance curve to another, but it is constant for a fixed (t_{Gi} - t_{Aci}) varying the chilled water temperature.
The two-phase flow in the generator is like to have an influence on the internal heat transfer coefficient. The experimental data show that this influence can be related to the strong solution flow rate.
It can be observed in Figure 4.10 that the UA value at the generator increases with increasing strong solution flow rate. The experimental correlation between the variables reads:

$$UA_G = (14.5\ m_s + 0.09) \tag{4.1}$$

4.6.2 Condenser

The condenser UA value is not constant varying the temperature thrust (t_{Gi} - t_{ACi}). Typical recorded data are shown in Figure 4.11.
The scatter of the points is very pronunced. In particular the data on the right hand side of the figure denote a higher UA value for (t_{Gi} - t_{Aci}) equal to 56 °C. These points are collected for experiments with a generator inlet temperature t_{Gi} equal to 85°C, while the points on the center and on the left hand side are for t_{Gi} equal respectively to 77 and 80 °C.
The reasons for this phenomenon are unclear. The heat transfer coefficient on both side of the tubes is not like to change in a relevant way during operation. Surely the typical condensation temperature, which ranges from 32 to 37 °C, is often above the room temperature. This can cause condensation on the external condenser wall. A lack of information on the quantity of refrigerant that could actually condensate out of the tube bundle, has led to the choice of employing directly the experimental data. The UA values are therefore averaged for each of the groups shown in Figure 4.11.

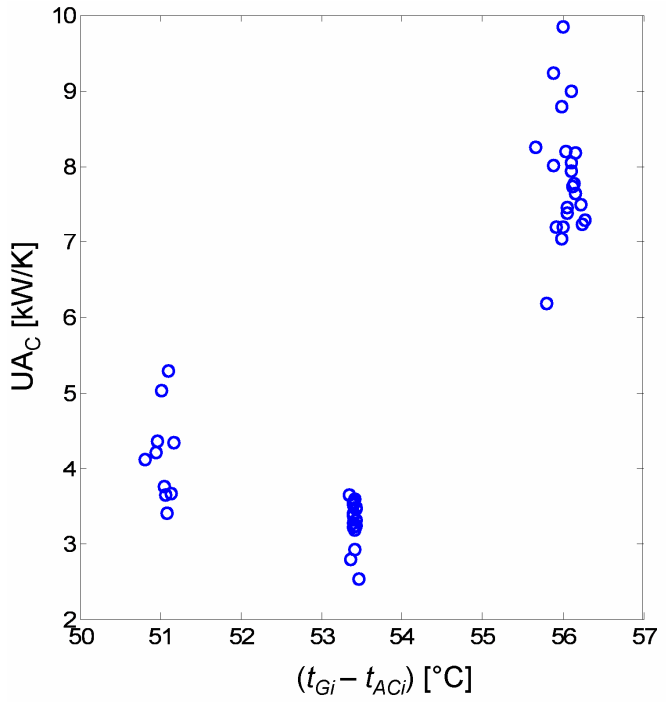

Figure 4.11 Condenser UA value for different values of the temperature thrust (t_{Gi} - t_{ACi})

4.6.3 Absorber

The absorber UA value could be retained fairly constant for various values of the temperature thrust. For the sake of simplicity the variations that can be observed in Figure 4.12 are not taken into account in the modeling and an average value is considered.

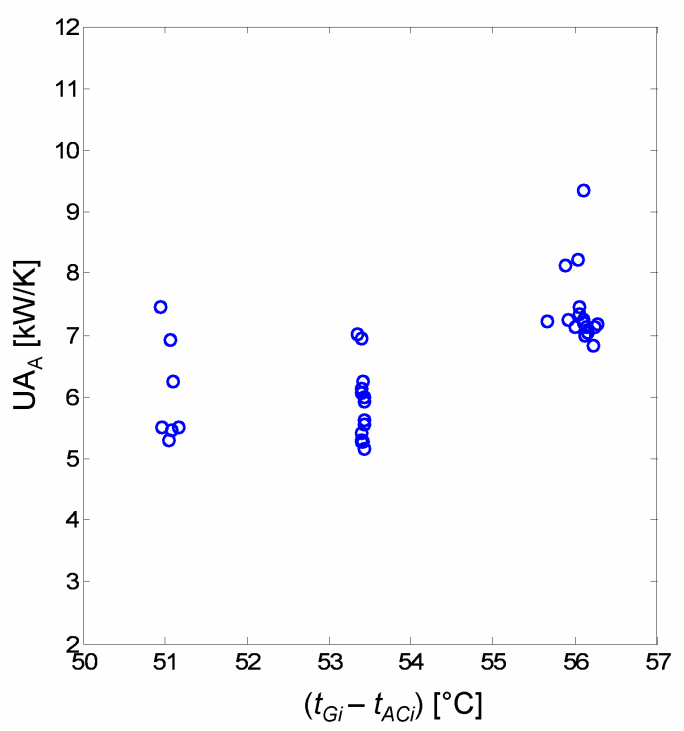

Figure 4.12 Absorber UA value for different values of the temperature thrust (t_{Gi} - t_{ACi})

From the knowledge of the absorber geometry the U value can be split in an internal heat transfer coefficient and an external heat transfer coefficient.
The usual equation for circular tube is:

$$U = \frac{1}{\left(\frac{D_o}{D_i}\right)\frac{1}{h_i} + \left(\frac{D_o}{D_i}\right)F_i + \left(\frac{D_o}{D_i}\right)\left(\frac{1}{2k}\right)\ln\left(\frac{D_o}{D_i}\right) + F_o + \frac{1}{h_o}} \tag{4.2}$$

For the calculation of the internal heat transfer coefficient the relation from Petukhov [Petukhov 1970] is used:

$$Nu = \frac{(f/8)\,Re_{D_i}\,Pr}{1.07 + 12.7(f/8)^{1/2}\left(Pr^{2/3} - 1\right)} \tag{4.3}$$

Where f is the friction factor and can be obtained from the Moody diagram or, for smooth tubes, from the following relation:

$$f = \left(0.790 \ln Re_{D_i} - 1.64\right)^{-2} \tag{4.4}$$

The resulting external (film side) heat transfer coefficient is determined experimentally and is in the range of 2.3 kW $m^{-2}K^{-1}$.

4.6.4 Regenerative heat exchanger

Not much information is available on the structure of the regenerative heat exchanger. It is a plate heat exchanger, probably built by the Yazaki itself. The UA value is observed to have a dependency on the internal flow rates. This means that it is not constant varying the temperature thrust. The dependency on the strong solution flow rate m_s is shown in Figure 4.13. The data can be fitted with a simple correlation between the UA value and the mass flow.

$$\mathrm{UA_R} = 9.79\, m_s \tag{4.5}$$

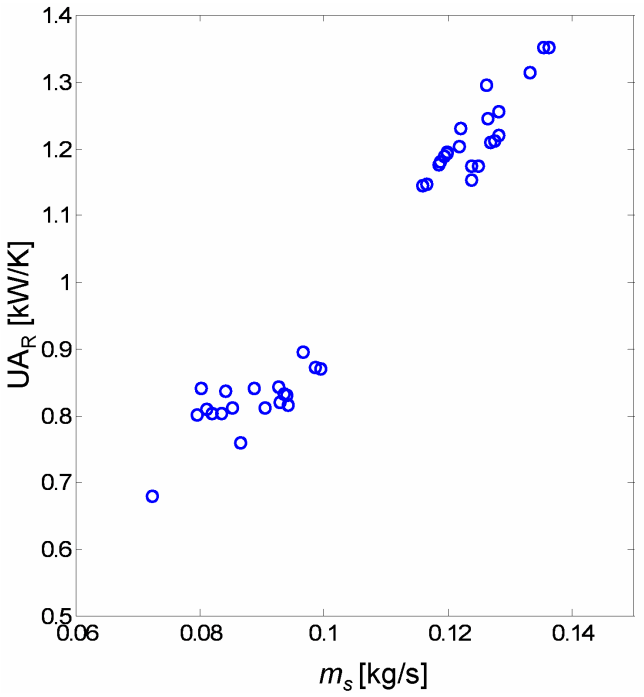

Figure 4.13 Variation of the regenerative UA value with the strong solution flow rate

4.6.5 Evaporator

The evaporator UA value is not constant for a fixed temperature thrust, as its value varies through the three curve domains; moreover it changes with the temperature thrust, having a dependency on the refrigerant flow rate.
As the heat transfer process at the evaporator has a remarkable influence on the performance of the WFC-10, it is here studied with some detail.
The evaporator heat exchanger is of the falling film type, with the refrigerant being distributed on the external surface of two concentric spiral coils. The chilled water flows in counter-flow inside the coils.

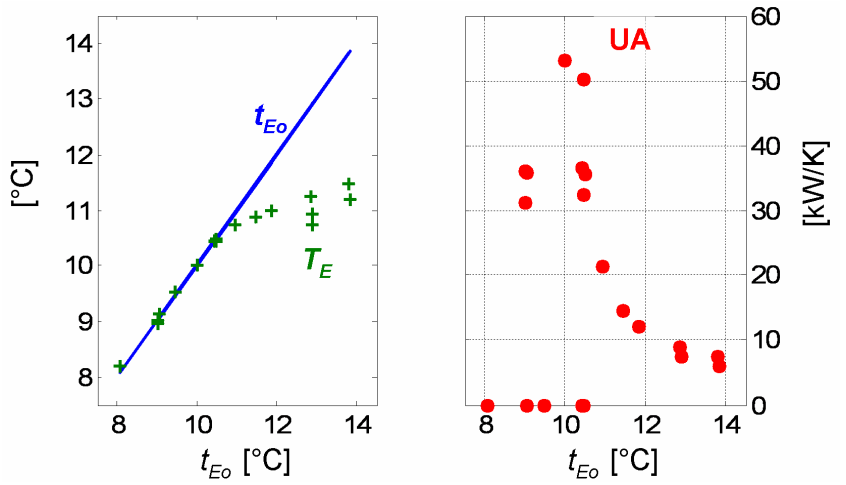

Figure 4.14 Temperatures at the evaporator and recorded UA values

Temperatures at the evaporator and UA values recorded for a fixed temperature thrust, with t_{Gi} = 85°C and t_{Aci} = 29.5°C, are reported in Figure 4.14. A specific measurement problem can be observed on the left hand side of the figure. Due to the low capacity the leaving chilled water temperature t_{Eo} is close to the evaporation temperature T_E. In some points the two temperatures overlap or the evaporation temperature is even greater than the outlet chilled water temperature. This has no physical sense, since the heat transfer occurs from the chilled stream to the evaporating refrigerant. The temperature differences are though so narrow that the accuracy of the PT-100 is not enough to give reliable results. The PT-100 are in fact guaranteed to have an uncertainty of 0.1 K. Some of the recorded temperature differences (t_{Eo} - T_E) are as small as 0.004 K with a standard combined uncertainty of ± 0.14 K. Therefore some of the UA values cannot be calculated and their uncertainty is very high.

The variation of the evaporator UA value through the three domains is illustrated in Figure 4.15. It appears that the UA value is decreasing in the second and third domain, because of a decreasing amount of evaporator area effectively wetted.

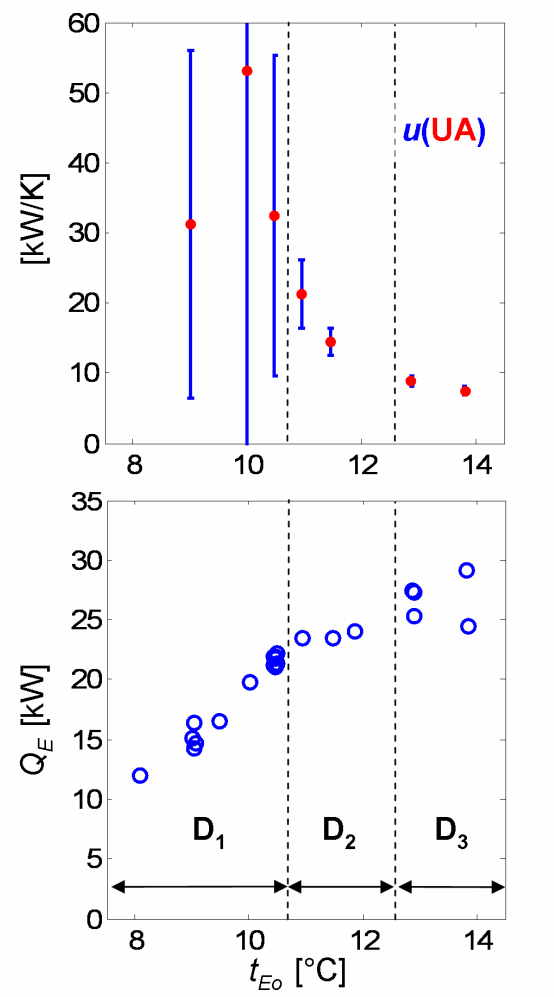

Figure 4.15 Uncertainty on the evaporator UA value

What happens in the first domain is on the other hand quite difficult to be determined. Some points suggest that the UA increases to a certain extent and then it starts to decrease.

To verify whether this hypothesis has some theoretical fundament the flow conditions and the heat transfer characteristics have to be analysed. The amount of refrigerant distributed on each coil is very low, in the range of 6 10^{-3} kg s^{-1}. The flow rate per unit length of one side of the tube is Γ = 0.001 kg s^{-1} m^{-1}.

According to the mode transitions of Hu and Jacobi [Hu and Jacobi 1996] the flow between each row is in form of droplets. The Γ value is so low that wettability problems of the coils are like to happen from the very first row of the tube bundle.

The internal heat transfer coefficient can be regarded as constant, since its variation with the temperature is not large. So, if one assumes that the overall wetted area of the evaporator cannot increase for increasing chiller capacity, the focus should be on the external (film side) heat transfer coefficient. Two reasons could lead to an increase of the heat transfer coefficient in domain 1.The first is inception of nucleate boiling, which causes the heat transfer coefficient to have dependence on the heat flux and on the driving temperature difference. Studies on nucleate boiling for water on copper at sub atmospheric pressure are rare. One proposed by Choon et alii [Choon et al. 2006] is applied to the present case to check if the working conditions can lead to boiling inception. As shown in Figure 4.16 the heat flux is variable through the tube bundle but is not high enough to justify a well developed nucleate boiling.

The second possibility for an increase in the external heat transfer coefficient is laminar flow with a decreasing film thickness. The flow is actually laminar, but as stated before, the evaporator is unevenly wetted. To have a systematic decrease of the film thickness the ideal case would be a constant portion of wetted area with a decreasing flow rate. No information on the flow pattern is available, but it seems due to the low flow that the film breaks down in rivulets with variable thickness. Moreover, the external surface of the coils is of the roll worked type. This type of tube has better heat transfer performance compared to the smooth one. But, more importantly, the influence of the flow rate on the heat transfer coefficient is different for this type of tubes. A work from Liu and Yi [Liu andYi 2002] reports on typical values and behavior of the heat transfer coefficient on roll worked tube bundle.

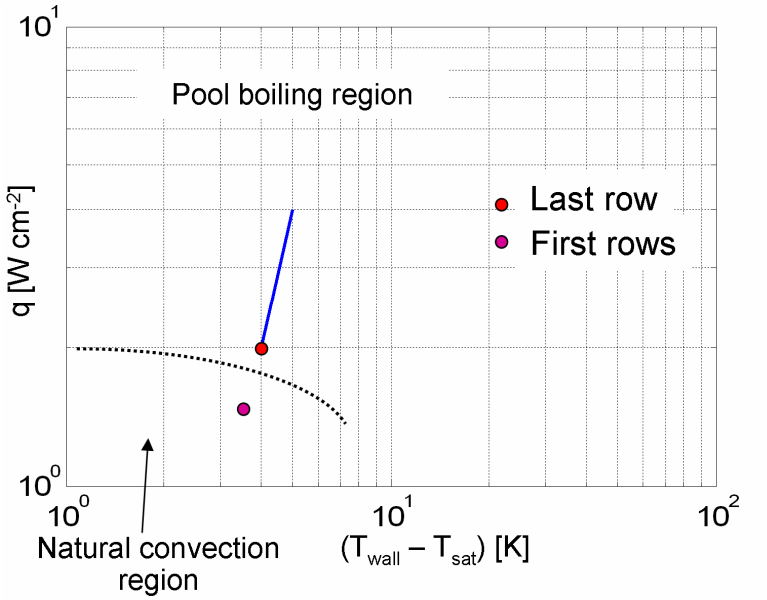

Figure 4.16 Inception of nucleate boiling for water on copper at sub atmospheric pressure (adapted from Choon et al. 2006)

As shown in Figure 4.17 there is a noteworthy difference between traditional and enhanced tubes. While for smooth tubes the flow rate in laminar conditions has effect on the α, for the reason of a varying film thickness, the same is not true for the roll worked tubes. The α remains constant in a wide range of flow rates, including the transition from laminar to turbulent flow. Conditions of the test are not identical to those of the WFC-10 evaporator and the tube surface can have slightly different characteristics, yet the results of Liu and Yi might be applied to the present case. The value of the external heat transfer coefficient confirms this hypothesis. The first UA value which is measured with good accuracy is around 20 kW K^{-1}. Knowing the heat exchanger surface and the internal heat transfer coefficient, an external heat transfer coefficient as large as 15 kW m^{-2} K^{-1} is necessary to obtain that UA value. So the heat transfer process is like to be strongly influenced by the enhanced tube surface.

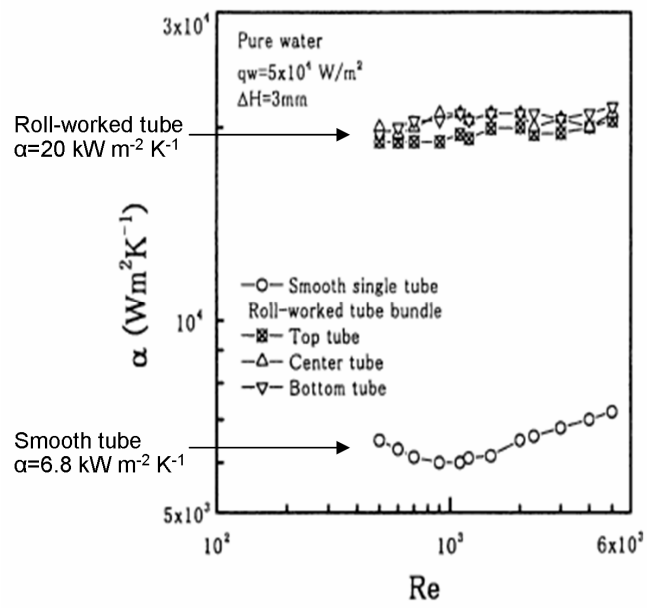

Figure 4.17 Falling film evaporation heat transfer coefficient on roll worked tubes (from Liu and Yi 2002)

4.7 Partially wetted evaporator modeling

From the previous discussion it turns out to be difficult to base the simulation of the evaporator heat exchanger on the experimental data. The uncertainty in the domain 1 of the performance curve is too high to find some sort of correlation between the UA value and other variables.

On the other hand it is important to include the variation of the exchanger wetted area in a general model of the WFC-10, to properly reproduce its typical performance. Therefore a model for the evaporator, based on few simple principles, has been developed.

The UA value is split in its internal and external heat transfer coefficient. The internal heat transfer coefficient is found from the relation (4.3) employed also for the absorber.

The external heat transfer coefficient is assumed to be constant, with a value of 15 kW m^{-2} K^{-1}, for the reasons outlined in chapter 4.6.5. The

employed area of the heat exchanger has to be related to the flow rate of the falling film.
Considering a row of the tube bundle a wettability function can be built up, where the wetted area depends on the film flow rate per unit length of one side of the tube Γ.
The fraction of the wetted area A_{fr} is:

$$\begin{aligned} A_{fr} &= 755.287\Gamma + 0.1224 \qquad for\ \Gamma \le \Gamma_{crit} \\ A_{fr} &= 1 \qquad\qquad\qquad\qquad\ for\ \Gamma > \Gamma_{crit} \end{aligned} \tag{4.6}$$

It has to be expected that the tube is completely wetted until the flow reaches a critical value Γ_{crit}. After that, the fraction of wetted area decreases with the flow rate (linearly is just a very simple assumption) and should reach zero for no flow rate. In the relation (4.6) the fraction of wetted area never reaches zero, even for Γ = 0. This contradicts a logical expectation, but it is done to ease the computation. If the A_{fr} approached the zero linearly with Γ the condition of a dry tube would be never verified. In fact the area available for the heat exchange becomes very small for small Γ values and the refrigerant would never be completely evaporated.
The relation (4.6) is applied to each row of the tube bundle for both the spiral coils, as shown in Figure 4.18. This gives the fraction of wetted area for each of 16 parts. The heat transfer rate equation (2.11) and two energy balances like equations (2.9) and (2.10) are simultaneously employed on each part, until the whole absorption model converge to a solution. If any refrigerant is left as liquid at the end of the tube bundle it goes to the absorber sump, where it is mixed with the weak solution. This happens in the domain 1 and 2 of the performance curve, where the driving temperature difference is not high enough to evaporate all the refrigerant.

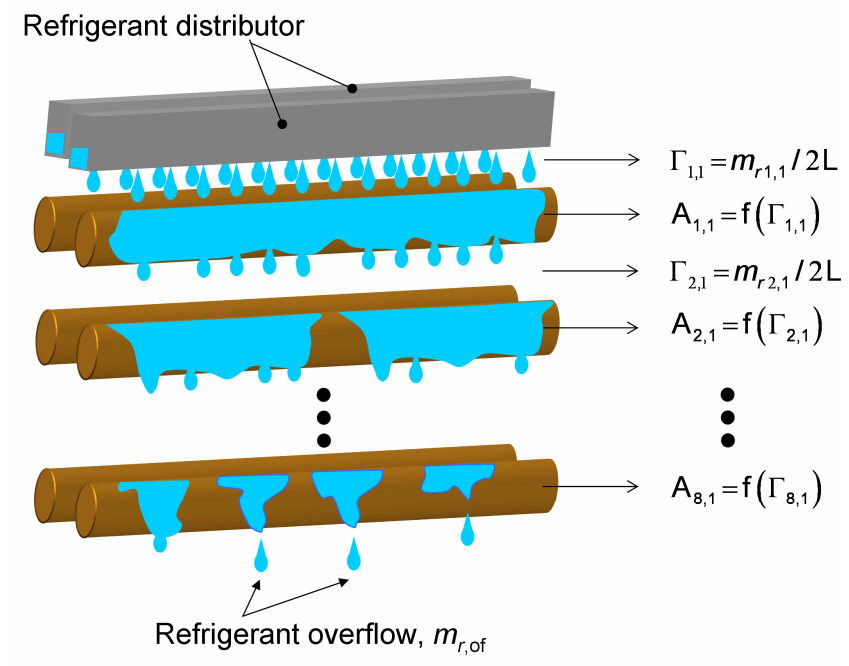

Figure 4.18 Calculation of the wetted area for each row of the tube bundle as a function of the refrigerant flow rate

4.8 Subcooling at the absorber outlet

A good amount of literature deals with the coupled heat and mass transfer process in the absorber. A comprehensive review of the published models was done by Killion and Garimella [Killion and Garimella 2001]. They point out that the hydrodynamics of the flow through the absorber are determining for its overall performance. Taking this suggestion Kyung et al. [Kyung et al. 2006] developed a former model of Kirby and Perez-Blanco [Kirby et al. 1994] in which three flow regimes are considered: 1) falling film regime over cooled tube, 2) drop formation regime at the bottom of the tube and 3) drop fall regime between the tubes. In the first regime as soon as the temperature profile begins to develop equilibrium conditions at the solution – vapor interface occurs, but due to the low mass

diffusivity the mass fraction boundary layer does not propagate deeply into the film. This leads to a remarkable subcooling of the solution, which is as high as 9 K in the Kyung's model (for the concentration, the pressure, the mass flow and the temperatures considered in the paper). During the drop formation highly subcooled portion of the film comes to the drop surface and promote high absorption flux. The heat of absorption brings the subcooling to lower values (in the order of 5 K). In the last flow regime no thermal and mass transfer effects are predicted. This theoretical analysis is applied to a tube bundle by the same authors and a final subcooling as high as 5.4 K is predicted at the absorber outlet. The verification of this result in an experimental rig [Kyung et al. 2006] has pointed out that the mass diffusivity value was a key parameter in tuning the model. The few data available on the mass diffusivity of lithium bromide solution are apparently too high according to the authors, and they make the model deviate from reality.

This overview shows how absorber models, due to their complexity and lack of well proved physical data on the mass diffusivity, are not easy to employ in a whole absorption model.

Nevertheless in the present work some preliminary simulations of the Yazaki WFC-10 chiller have shown that the assumption of no subcooling at the absorber outlet causes the capacity to be over predicted at low values of the chilled water temperature. It is interesting to note that a subcooling as little as 2 K in the weak solution leaving the absorber leads to 4.5 kW less capacity compared to the case of no subcooling. Good experimental verification of subcooling is not an easy task. In the WFC-10 test rig (see Figure 4.4) no temperature probe is positioned on the absorber tube bundle. The first available temperature of the weak solution leaving the absorber is at the entrance of the regenerative heat exchanger; here the solution temperature results from the mixing of the solution with the refrigerant overflow (see chapter 4.4). So to describe the state of the solution the lithium bromide mass fraction, the refrigerant overflow, the refrigerant and the solution temperature should be all known with high accuracy. In the present case the experimental analysis couldn't give reliable results on the presence of subcooling. On the other hand what would be very useful is not only the evidence of this phenomenon, which is like to take place often in an absorption chiller, but how it changes varying the working conditions. The analysis of a single performance

curve, like the one depicted in Figure 4.6, shows that the refrigerant flow rate and the weak solution flow rate do not vary significantly along the curve. From experiments and modeling also the two concentrations show very small variations. What surely changes with the chilled water outlet temperature is the evaporation temperature, i.e. the pressure level in the evaporator and the absorber. A paper from Matsuda et al. [Matsuda et al. 1994] points out that the pressure level in the absorber has an influence on the absorption rate, decreasing with decreasing pressure. It could be expected that the lower ability of absorbing vapour at low pressures can lead to a higher degree of subcooling. Although this is has not proved consistently in the literature so far, it fits with the impression had in running some simulations that the subcooling at low evaporation temperature should be higher than at higher temperatures.
A very simple fit was applied to the prediction of the subcooling in the absorber of the Yazaki, with the evaporation temperature as a parameter. The relation is:

$$subcool = 0.069 T_E^2 - 1.8808 T_E + 12.62 \quad [°C] \tag{4.7}$$

4.9 Assumptions of the WFC-10 model

The assumptions of the WFC-10 absorption chiller model are basically those outlined in chapter 2.3. Few of them are reviewed, as they would lead to unrealistic prediction of the chiller performance.

1) Steady state conditions
2) The pressure in the condenser is equal to that of the generator; the pressure in the evaporator is equal to that of the absorber
3) Pressure changes occur only in the expansion valves and in the pump, there are no head losses along the tubes
4) No heat losses to the environment
5) Heat exchangers UA values depend on working conditions
6) Weak solution flow rate depends on working conditions
7) The refrigerant leaves the condenser and the evaporator respectively as saturated liquid and saturated vapour. If it is not entirely evaporated, it leaves the evaporator as a liquid overflow

8) The strong solution leaving the generator is assumed to be in saturated state. A certain degree of subcooling of the weak solution leaving the absorber is considered
9) The superheated steam leaving the generator has the temperature of the saturated strong solution leaving the generator

4.10 Model results

An evolution of the model presented in chapter 2 is employed for the simulation of the WFC-10. The major characteristic of this model is the inclusion of a more detailed section for the heat transfer phenomena. This includes experimental correlations for the variation of the UA value in the generator, condenser and regenerative heat exchanger.
At the absorber the external (film side) heat transfer coefficient is considered constant and detected from experimental data. For the evaporator a specific model is implemented, taking into account the distribution of refrigerant on the tube bundle as well as the change from an overflowing to a partially dry evaporator.
Three performance curves are chosen to compare the experimental data to the modeling results. The curves are given for different pairs of temperatures t_{Gi} and t_{Aci}, with a variable chilled water outlet temperature t_{Eo}.
Figure 4.19 shows the ability of the model to represent the performance of the WFC-10. The agreement with the experimental data is quite good. From the calculation the domain 3 of the curve results in a straight line. Here the last rows of the evaporator tube bundle are running dry. To check how the evaporator model works, the calculated evaporation temperature T_E and the UA value are reported in Figure 4.20
Figure 4.20. In the experimental data the evaporation temperature starts to level off earlier than in the model. There is also a difference in values, which is not significant. The UA value should be checked especially on the right hand side of the figure. As explained in chapter 4.6.5 the uncertainty in the measurement is too high in the domain 1 of the curve to draw reasonable conclusions. What is interesting is that the model is able to predict the decreasing behaviour of the UA value. The drop in the UA value appears for lower t_{Eo} in the experiments, like the stabilization of the

evaporation temperature T_E. Moreover all the UA values seem to be overpredicted by the model.
Other two groups of figures are presented in the following, to assess the validity of the model in simulating the characteristic behaviour of the WFC-10. The comments given for Figure 4.19 and Figure 4.20 hold true for the upcoming results.

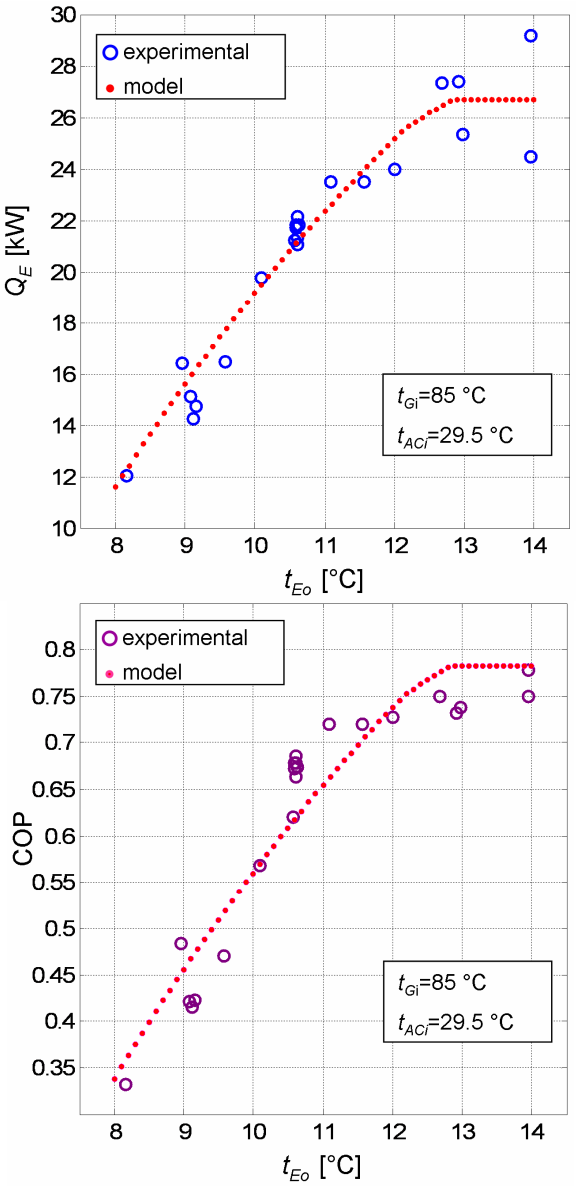

Figure 4.19 Capacity and COP predicted by the model for t_{Gi}=85, t_{ACi} = 29.5 °C and different values of the chilled water outlet temperature t_{Eo}

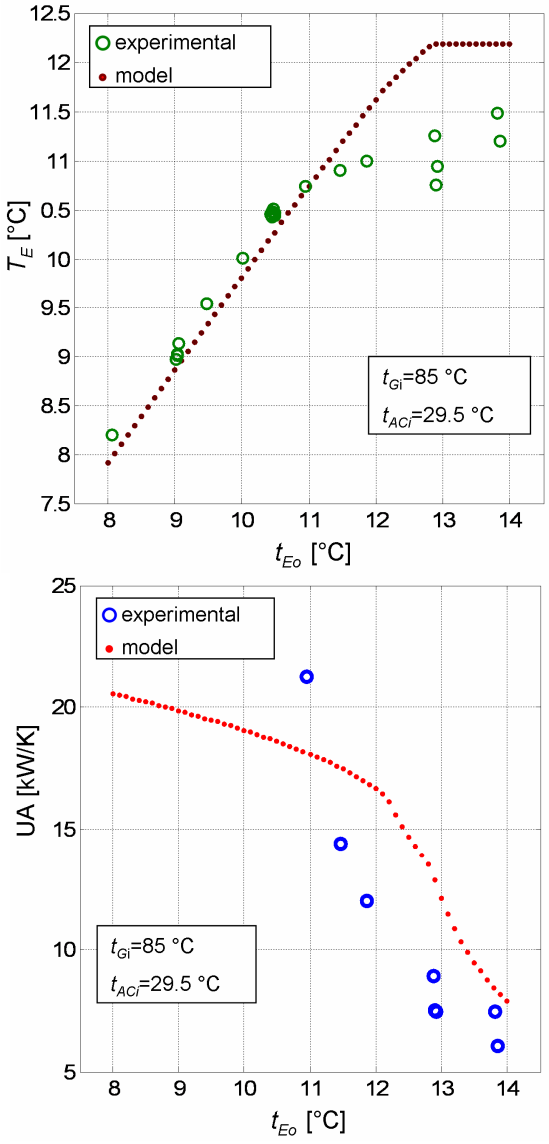

Figure 4.20 Evaporation temperature and evaporator UA value predicted by the model for t_{Gi}=85, t_{Aci} = 29.5 °C and different values of the chilled water outlet temperature t_{Eo}

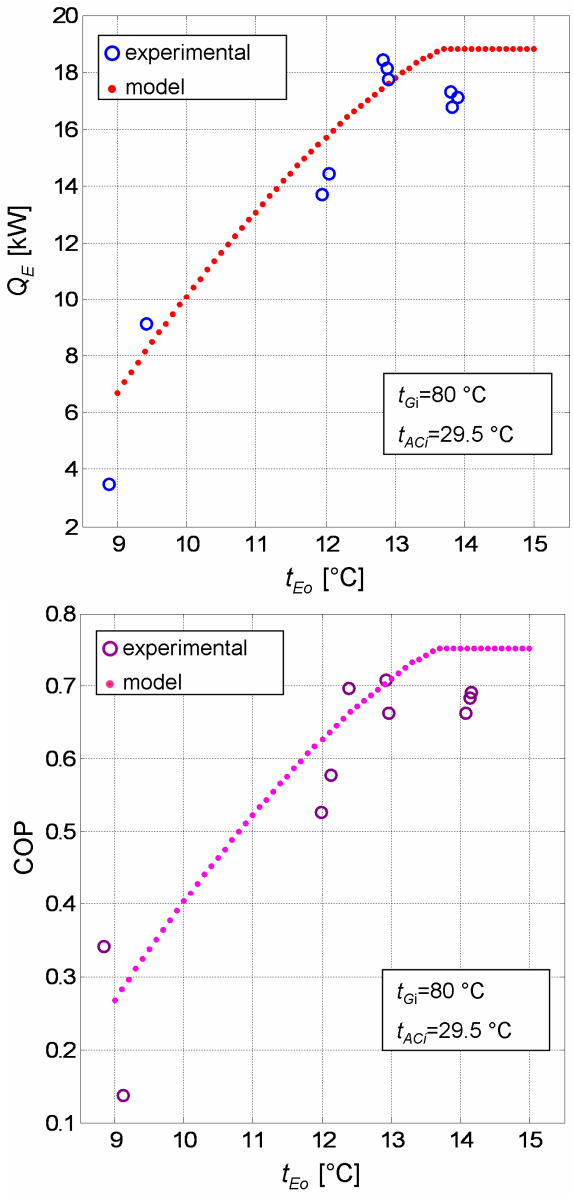

Figure 4.21 Capacity and COP predicted by the model for t_{Gi}=80, t_{Aci} = 29.5 °C and different values of the chilled water outlet temperature t_{Eo}

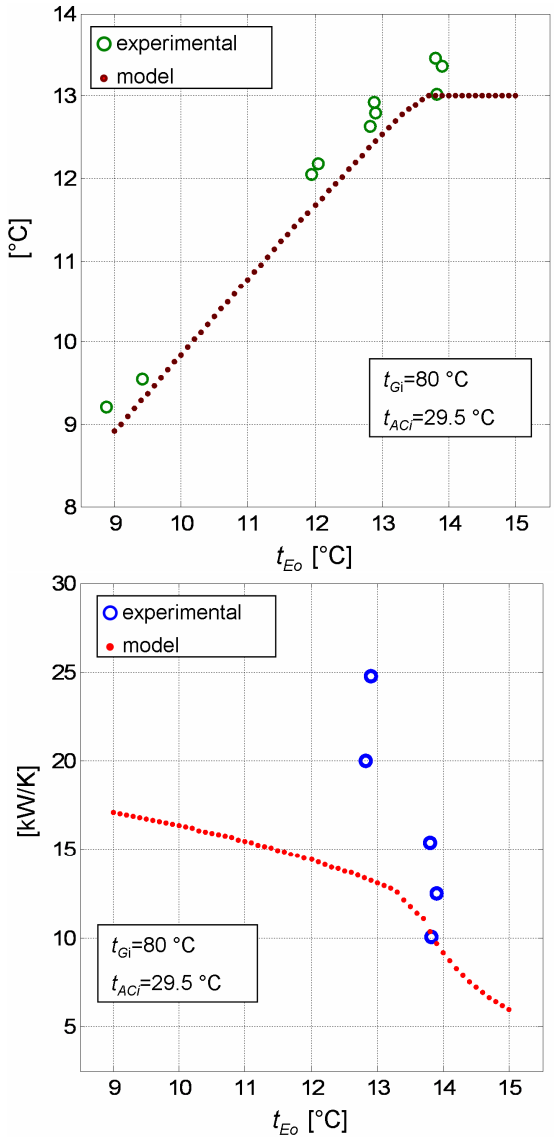

Figure 4.22 Evaporation temperature and evaporator UA value predicted by the model for t_{Gi}=80, t_{Aci} = 29.5 °C and different values of the chilled water outlet temperature t_{Eo}

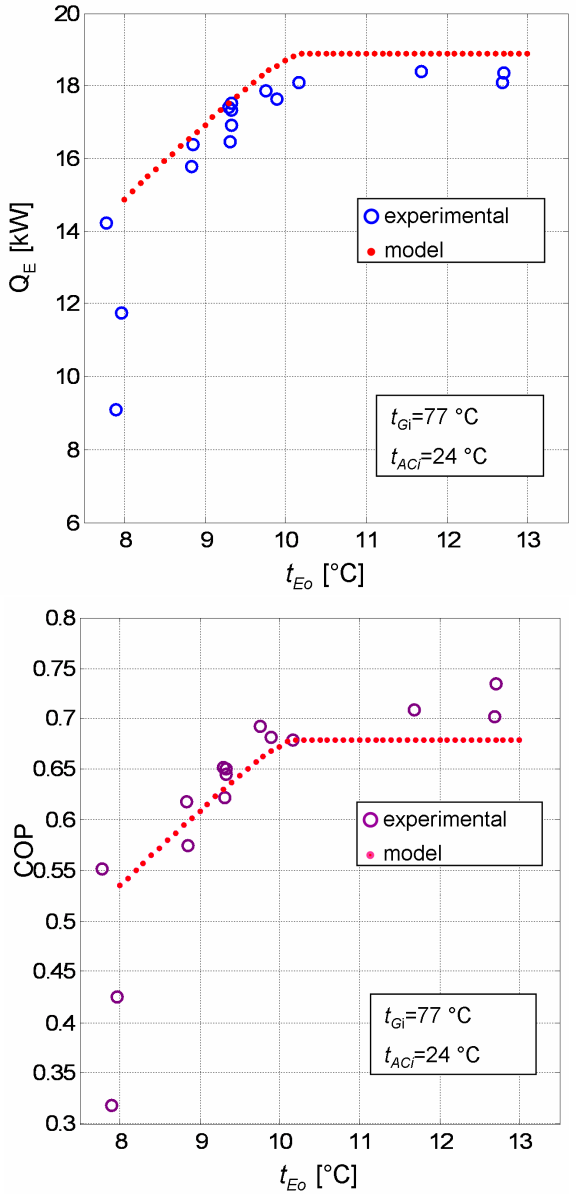

Figure 4.23 Capacity and COP predicted by the model for t_{Gi}=77, t_{ACi} = 24 °C and different values of the chilled water outlet temperature t_{Eo}

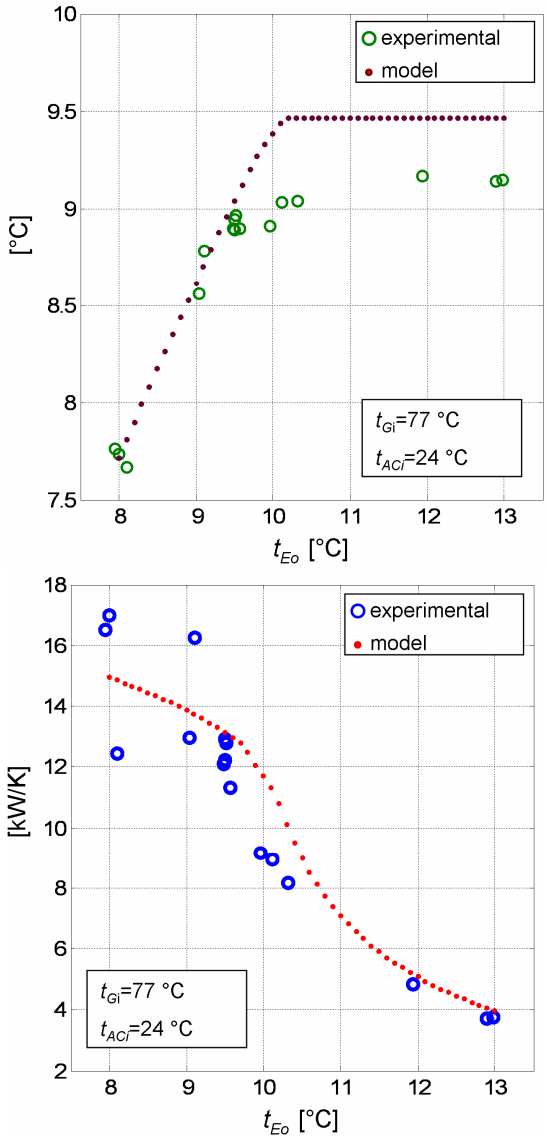

Figure 4.24 Evaporation temperature and evaporator UA value predicted by the model for t_{Gi}=77, t_{Aci} = 24 °C and different values of the chilled water outlet temperature t_{Eo}

5 Solar cooling system design

5.1 Solar cooling system

A solar cooling system is made of different components. In Fig. 1 a general scheme is shown. The cooling demand can be satisfied by the absorption chiller, the compression chiller or the cold storage. The thermal power needed by the absorption chiller is supplied by the solar collector field, the auxiliary heater or the hot storage. Cooling towers for the chillers heat rejection complete the scheme. In order to reduce the plant complexity (and the cost of the system) some simplified configurations can be drawn.

In the simplest solar cooling plant (1 + 4 + 7) all the thermal load is satisfied by a totally solar driven absorption chiller. In this case, the absorption chiller has to be sized with respect to the pick demand ($Q_E \geq Q_{L,\max}$). The solar collector field must be oversized, because it has to drive the chiller also during the periods of low irradiation ($Q_{Coll} \geq Q_G$). So for a long time the heat collected is wasted. Clearly, this is not an optimized system both from the energetic and economic point of view.

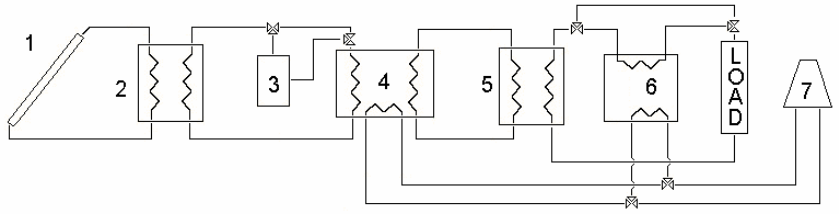

Figure 5.1 Scheme of a solar cooling plant: 1 = solar collector field; 2 = hot storage; 3 = auxiliary boiler; 4 = absorption chiller; 5 = cold storage; 6 = compression chiller; 7 = cooling towers

In order to avoid wasting the heat collected, a hot storage can be inserted between the solar field and the absorption chiller (1 + 2 + 4 + 7). The storage capacity must be evaluated by matching the thermal power produced by the collectors and the chiller heat demand. When $Q_{Coll} > Q_G$, the heat surplus is stored in the tank; when $Q_{Coll} < Q_G$, the hot storage is

needed to drive the absorption chiller: this situation typically occurs at the beginning and at the end of the day, when the solar radiation level is not high enough to drive the chiller at its lowest capacity. The collectors area is partially reduced with respect to the previous case: in fact, when the irradiation is low, the hot storage can contribute to supply the chiller generator.

To significantly reduce the collectors area, an auxiliary boiler could be introduced (1 + 3 + 4 + 7). In this case, a fraction of the energy input to the generator can be supplied by the burner. The heat collected by the solar devices is wasted for few time, when the building load is low and the solar radiation is high ($Q_{Coll} > Q_G$). Ziegler et alii [Ziegler et al. 2006] have demonstrated that if the solar cooling system is integrated with a traditional burner to supply the generator in periods of scarce solar radiation, the solar fraction, i.e. the quantity of energy input to the generator from solar collectors divided by the total energy delivered to the generator, should be in general well above 0.5 to achieve primary energy saving in comparison with a compression chiller system. It is evident that the use of a burner to integrate the energy input to the generator could have advantages on the initial cost of the system but not on the final primary energy demand. If the cooling effect Q is to be obtained with the burner and the absorption chiller, an energy input equal to $Q/(\eta_b\ COP_{abs})$ is required, while the compression chiller would require $Q/(\eta_{el}\ COP_{comp})$. For a mean efficiency of the electrical power generation and distribution with the best available technologies $\eta_{el} = 0.5$, of the burner $\eta_b = 0.9$, of the absorption chiller $COP_{abs} = 0.7$ and of the compression chiller $COP_{comp} = 4$, the burner requires three times the energy input of the power plant. This explains the need to minimise the auxiliary energy demand with systems having high solar fractions.

The auxiliary boiler could be introduced also in a solar cooling plant with hot storage (1 + 2 + 3 + 4 + 7). In this case the heat collected is never wasted, because when it occurs that $Q_{Coll} > Q_G$ the heat can be stored. Nevertheless, the above considerations about the primary energy consumption in presence of traditional burner are again consistent.

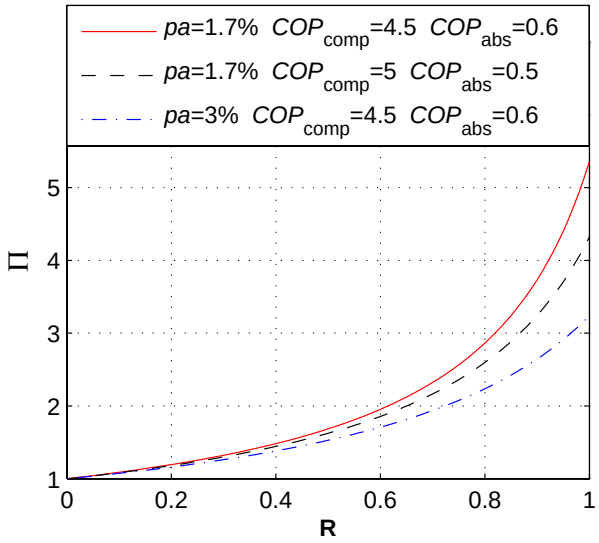

Figure 5.2 Ratio between PE_{comp} and $PE_{comp+abs}$ as a function of the load fraction covered by the absorption chiller R, for different values of pa, COP_{comp} and COP_{abs}

The use of a cold storage (1 + 4 + 5 + 7) could allow a slight reduction of the absorption chiller capacity, because the pick of the cooling demand could be satisfied by the cold storage. Nevertheless, the (only solar driven) absorption chiller could not operate at nominal capacity because of low radiation. So it could be that the chiller capacity is undersized with respect to the pick load ($Q_E \leq Q_{L,max}$), but considerations about thermal load profile and solar radiation availability are needed for sizing the absorption chiller and the cold tank. In comparison with the hot storage, the cold one has some advantages: the losses to the environment occur under a smaller temperature difference (in the order of the 15°C, against the 50°C of the hot storage); to bring the tank in its operative conditions during the start up or after a long idle period requires less energy (assuming that the tank is in equilibrium with the environment); the energy to be stored when $Q_E > Q_L$ is only ($Q_E - Q_L$) while for the hot storage it would be ($Q_E - Q_L$)/COP_{abs}.

The integration of the absorption chiller in the traditional cooling system based on compression chiller (1 + 4 + 6 + 7) has the advantage that any load not covered by solar energy is met by the compression chiller, avoiding the use of a back up burner. Further more when the two chillers work together, the major part of the control effort can be overtaken by the compression chiller, varying the electrical input to the compressor. The primary energy consumption for the system operating with the compression chiller only is:

$$PE_{\text{comp}} = \frac{\mathrm{Q}_L}{\eta\, COP_{\text{comp}}} + pa\,\frac{\mathrm{Q}_L\left(1+COP_{\text{comp}}\right)}{\eta\, COP_{\text{comp}}} \tag{5.1}$$

where Q_L is the energy required by the load, *pa* is a coefficient expressing the electrical consumption of the cooling towers as a fraction of the total heat rejected. Considering the typical operation temperature of a single stage absorption chiller, usually wet cooling is employed. A value for *pa* equal to 1.7 % is found relating the electrical consumption of some commercial cooling towers to their nominal capacity. The primary energy consumption for the traditional system integrated with the absorption chiller is:

$$PE_{\text{comp+abs}} = \left(1-R\right)PE_{\text{comp}} + pa\,\frac{\mathrm{Q}_L\, R\left(1+COP_{\text{abs}}\right)}{\eta\, COP_{\text{abs}}} \tag{5.2}$$

where *R* is the fraction of the load covered by the absorption chiller ($\mathrm{Q}_E/\mathrm{Q}_L$). To have primary energy saving the ratio Π between PE_{comp} and $PE_{\text{comp+abs}}$ should be greater than one.

As shown in Fig. 2, Π is strongly influenced by the *pa* value, while it is less dependent on the *COP* of the compression and of the absorption chillers. The integration of the solar assisted absorption chiller in the traditional system has always an environmental benefit, even for small values of *R*.

The highest flexibility can be obtained if also a cold storage is integrated into the plant (1 + 4 + 5 + 6 + 7): so the system can be regulated both by means of compression chiller and cold storage. Energy waste does not

take place. The surface of solar collectors can be sized with respect to the maximum of solar radiation $G_{t,\max}$ and the capacity of the absorption machine:

$$A_{Coll} = \frac{Q_{E,\max}}{\eta_{Coll}\, G_{t,\max}\, COP_{abs}} \tag{5.3}$$

The solar driven chiller operates following the irradiation availability, so it does not ever occur that $Q_{Coll} > Q_G$. When $Q_E > Q_L$, the surplus of chilled water is stored.
The solar cooling system integrated with compression chiller could be finally completed with the hot storage (1 + 2 + 4 + 5 + 6 + 7), to obtain extreme flexibility on the sizing of its elements.

5.2 System design approach

A solar cooling system usually replaces or integrates a conventional one. As a matter of fact an investor that chooses this kind of system has high expectations for energy savings and economic convenience. While as outlined in chapter 5.1 solar thermal cooling can lead to primary energy savings, the economic convenience is not so easy going. The initial investment might be too consistent to be repaid within the life of the system. A proper design method has to deal with that, otherwise the spread of this technology will remain very limited.
In this work the design approach is of the type simulation-optimization. Several simulations of a complete system are carried out changing the main design variables until an optimum value of an objective function is found out. Aim of the optimization is to maximise the solar savings of the system, defined as the difference between the cost of a conventional system and a solar system [Duffie and Beckman 2006]. A step of the design process is therefore the definition of two system configurations, the conventional and the solar one. This doesn't affect the generality of the method, as long as different reference systems can be considered. On the other hand the cost minimization of a solar cooling system on its own wouldn't give any information on the economic competitiveness of this technology.

Although the major effort of this work is to optimize the design of a solar cooling system, the employment of solar collectors during winter time is also considered. Therefore the optimal size of all the components is searched considering the all year operation of the system.

5.3 System configuration and design variables

The arguments drawn in chapter 5.1 show that a possible configuration of the solar cooling system includes the elements reported in Figure 5.1, except the auxiliary burner. The cooling load is satisfied by the cold storage. If the temperature is not low enough the compression chiller works in series to the storage.
The conventional system, chosen here as a reference, consists on the other hand of the load, the cooling towers and a compression chiller.
In winter time the solar system partially satisfies the heating demand. The solar collectors preheat a thermal storage, from where water is taken and further heated up to the required temperature by a conventional gas burner. The reference system is in this case made up of the gas burner only. Figure 5.3 summarises the configurations and their usage during the cooling and the heating season.
Once the load is fixed, the main design variables of the solar cooling system are: the orientation of the solar collector array (slope and azimuth), the collector area A_{Coll}, the chiller capacity $Q_{E,nom}$, the volume of the hot storage V_h, the volume of the cold storage V_c, the capacity of the back up compression chiller $Q_{comp,nom}$, the capacity of the cooling towers Q_{tower}.

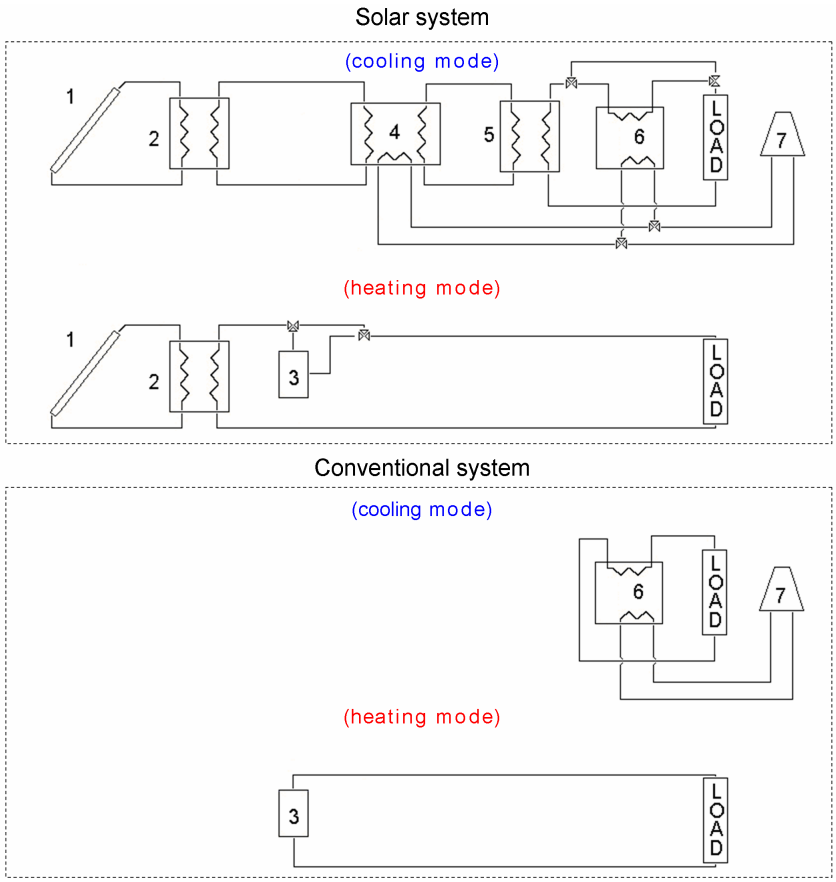

Figure 5.3 Solar and conventional system configurations

Not all these variables are included in the optimization. The orientation of the solar collectors for instance is determined once to maximize the energy collected during the whole year. This can be a reasonable choice for a system which exploits solar energy both in winter and summer. The capacity of the compression chiller is related to the other variables, in fact it depends on what part of the cooling load is not covered by the absorption chiller and the cold storage. Finally the capacity of the cooling towers is determined by the sizes of the two chillers. In the end the optimization process is carried out on four variables, which are the solar

collectors area A_{Coll}, the capacity of the absorption chiller $Q_{E,nom}$, the volume of the two thermal storages V_h and V_c; the other variables are calculated consequently to match the load and the heat rejection requirement.

5.4 Simulation and optimization

The performance of each system is calculated by simulation. The TRNSYS environment has been employed for this purpose [Klein et alii 1996].

TRNSYS has a standard library of components that includes most of the elements usually employed in HVAC installations. To model the absorption chiller the code described in the first chapters of this work has been used. The part load behaviour of the cooling towers and of the compression chiller is simulated thanks to two standard components of TRNSYS which rely on performance data supplied by the user.

To perform the design optimization an external program has to adequately change the variables and launch several TRNSYS simulations. This is done by means of the generic optimization tool GenOpt, developed at the Lawrence Berkley National Laboratory [Wetter 2004]. GenOpt can be interfaced with any other software that reads input data from a text file. A scheme on how the communication between TRNSYS and GenOpt takes place is shown in Figure 5.4.

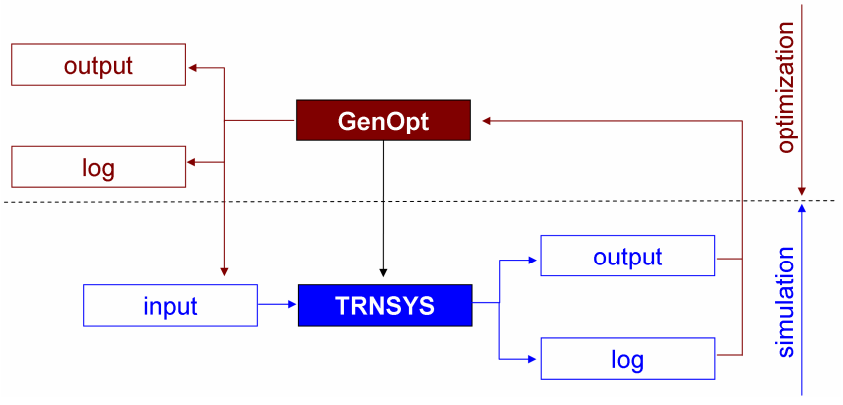

Figure 5.4 Interface between GenOpt and TRNSYS

GenOpt has to solve the optimization problem:

$$\begin{aligned} &\max S(\bar{x}) \qquad && \bar{x}=(Q_{eva}, A_{coll}, V_h, V_c) \\ &\bar{a} \le (\bar{x}) \le \bar{b} \end{aligned} \tag{5.4}$$

Where S are the solar savings of the system:

$$S = C_{conv} - C_{solar} + \sum_{i=1}^{20} \left(PW_i \left(CF \right) \right) \tag{5.5}$$

The terms in the (5.5) are the initial cost of the conventional system C_{conv}, the initial cost of the solar system C_{solar}, and the present worth of the difference between the operation cost of the conventional and the solar system evaluated for 20 years of operation. If S is positive, it means that it is convenient on that time horizon to purchase the solar system. Typically the investment for a traditional system C_{conv} is smaller than C_{solar}, while the yearly net cash flow CF is a positive value.

5.5 Test case

To show how the optimization-simulation procedure works, a planning case is here presented. The building under consideration is part of the Department of Industrial Engineering of the Bergamo University; it is a three floors building with a $11 \cdot 10^3$ m^3 total volume. The optimization is carried out for two different Italian sites: Bergamo and Rome. This should give an idea on how different locations lead to different optimized systems. The thermal loads of the building are calculated with TRNSYS type 56, a component of the TRNSYS library able to predict the transient behaviour of a multizone building. The thermal demand during the year is shown in Figure 5.5.

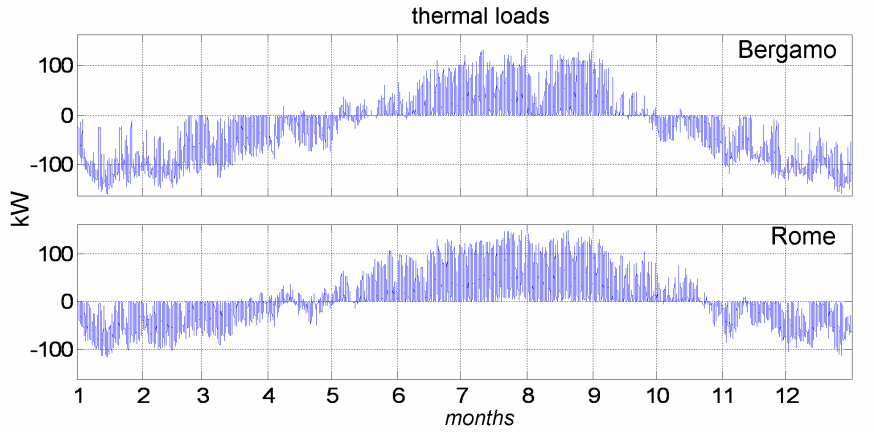

Figure 5.5 Power required for heating and cooling a three floors building of the Bergamo University

The total energy required for heating and cooling is reported in Table 5.1. A different share of the year load is observed in the two cases. For Bergamo 80 % of the entire energy requirement is needed for heating purpose, for Rome the load is equally divided in heating and cooling demand.
The orientation to maximize the solar energy collected on the array surface is shown in Table 5.1.

	Bergamo	Rome
Heating load	$1.21\ 10^6$ MJ	$5.02\ 10^5$ MJ
Cooling load	$2.96\ 10^5$ MJ	$5.14\ 10^5$ MJ
Collector orientation	slope 32°, az. 0°	Slope 34°, az. 1° O
Solar Energy	$5.17\ 10^3$ MJ/m^2	$6.64\ 10^3$ MJ/m^2

Table 5.1 Yearly loads, optimized collector orientation and yearly collected solar energy for the two installation sites

The slope and the azimuth are not very different for the two sites, which suggests that in Rome a considerable part of the solar energy is collected during winter also. The energy collected in Rome is nearly 30% more than the one collected in Bergamo. Solar radiation distribution through a year is reported in Figure 5.6.

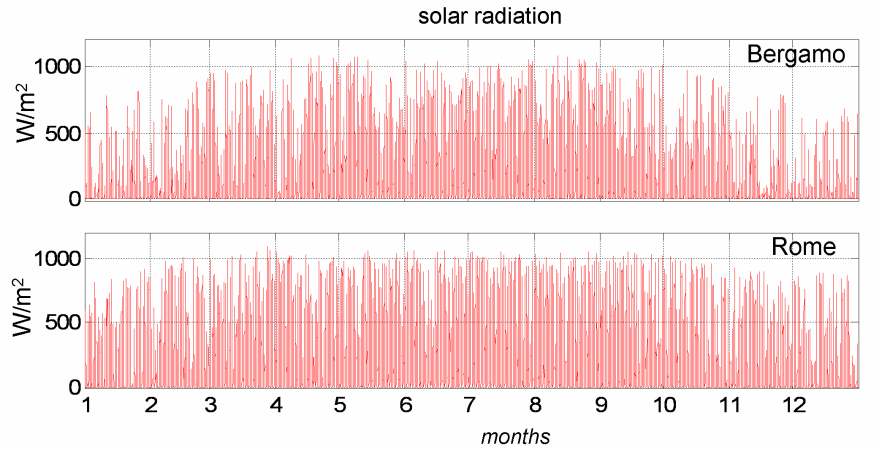

Figure 5.6 Solar radiation on collector surface in the two sites

5.5.1 Thermal system details

Many choices influence the overall performance of a thermal system simulated with TRNSYS. They are mainly of two kinds: type of components employed in the simulation; control strategy of the system.
As previously mentioned the absorption chiller is here simulated with the model presented in chapter 2. The characterization of the chiller, in terms of distribution of the heat exchange area between the components and the typical internal flows, is made referring to the performance of the Thermax chiller presented in chapter 3. So, the discrete values of the chiller size explored during the optimization correspond to different sizes of the Thermax chiller. Nevertheless the chiller capacities available on the market are a limited set of discrete values, ranging from 70 to more than 2000 kW. To have more freedom in the optmization procedure, two ideal

hypothese are made: the sizes of the chiller are discretized with a 5 kW step, the capacity of the chiller ranges from 0 to 150 kW. Therefore the optimization can give a nominal size of the absorption chiller which is actually not on the market. On the other hand it is preferred to find an ideal size, keeping in mind that other chiller manufacturers and sizes can be considered afterwards.
The compression chiller is modeled according to typical performance data of the Carrier 30HWC series. This is a water cooled, reciprocating chiller, employing R-22 as refrigerant. It has a COP in the range of 4, depending on working temperatures and size.
The wet cooling tower is modeled referring to typical performance data of the Evapco ICT series.
The solar collectors considered are of evacuated type, model Solamax 30 from the Thermomax company. Their second order efficiency curve is obtained from the standard certification performed by the SPF Institut in Rapperswil. Others components relevant for the system modeling are the thermal storages. They are modeled with TRNSYS standard component type 4. To take into account the thermal stratification the storages are divided in 10 fully mixed segments. The losses from the tanks to the environment are calculated with an overall heat transfer coefficient equal to 0.8 W $m^{-2}K^{-1}$.
The control strategy of the system is quite simple. The cooling load has to be satisfied with water at 7 °C. The chilled water returns from the load at 12.6 °C. To match the load the chilled water flow rate in the fan coils is continuosly adjusted. This allows to keep the inlet and outlet fan coils temperatures constant. The chilled water is always taken from the cold storage, when its temperature is greater than 7 °C the compression chiller is used in series to the storage.
The solar collectors heat up the hot storage. Water from the top of the storage is sent to the generator of the absoprtion chiller. The start up temperature of the chiller is set to 72 °C. All the chiller capacity is used to cool the cold storage.
During winter the solar collectors heat up one of the two thermal storages. It is the cold or the hot one depending on which has the larger volume. Usually from the optimization the cold one results to be the largest and is therefore employed in winter. This is not clearly shown in Figure 5.3. Moreover is a configuration which assumes that the piping and the valves

allow to actually use one of the two thermal storages indifferently. The heating load is satisfy with water at 60 °C. The water returns from the heating system at 40 °C. Again, like for cooling, the load is followed varying the flowrate in the circuit and not the temperatures. Water is always taken from the storage and further heated up, if necessary, by the traditional gas burner. As can be noted the system control strategy is kept very simple to avoid complications in the simulation. Of course different system configurations and control strategies can be analysed, leading to different system performance. This is though beyond the scope of the present investigation.

5.5.2 Economic parameters

Since the objective function of the optimization is an economic value, definition of the installation and running costs is of primary importance.
The installation cost of the absorption chiller is assumed to be size dependent. The following exponential relation is used for size up to 100 kW. For bigger chiller a constant cost of 500 €/kW is assumed.

$$\begin{aligned} &C_{abs,chiller} = 4396.2\, Q_{E,nom}^{-0.48} \\ &10 \le Q_{E,nom} \le 100\,\text{kW} \end{aligned} \tag{5.6}$$

The cost for small chillers is not well defined yet, as they are still entering the market, but the (5.6) gives a good approximation.
The cooling tower has also a size dependent cost. The relation is:

$$C_{tower} = -0.0368\, Q_{tower,nom} + 36.42 \tag{5.7}$$

The (5.7) can be employed for installed tower capacity up to 400 kW. The other installation costs are reported in Table 5.2 together with the running costs. In the analysis of the primary cost an important subsidy available in Italy has been considered. In fact an incentive to the use of solar thermal collectors has been introduced with the financial law 296/2006. The 55% of the initial investment is deductible from taxes during a period of three years, till a maximum total amount of 60 k€. Some preliminary calculations [Franchini, Nurzia and Perdichizzi 2007] have shown that the

subsidy is essential to enhance the economic competitiveness of the solar cooling system.

Primary costs	
Absorption chiller	500-1500 €/kW_{th}
Compression chiller	200 €/kW_{th}
Cooling towers	21.7-36 €/kW_{th}
Solar collectors	400 €/m^2
Thermal storage	600 €/m^3
Running costs	
Electricity	0.2 €/kWh
Natural gas	0.55 €/m^3
Water	1 €/m^3
Present worth figures	
Life time	20 years
Discount rate	0.033
Inflation rate	0.04

Table 5.2 Economic parameters

5.6 Optimization results

The algorithm chosen to run the optimization with GenoOpt is of the Pattern Search type, it can be applied to either problems with continuos or discrete variables. The procedure finds out a solution to the optimization problem after 163 simulations. The final values that maximize the solar savings of the systems are reported in
Table 5.3.

	Bergamo	Rome
$Q_{E,nom}$	45 kW	70 kW
$Q_{comp,nom}$	90 kW	90 kW
A_{Coll}	164 m^2	202 m^2
V_h	10 m^3	8 m^3
V_c	14 m^3	18 m^3

Table 5.3 Optimized sizing of the solar cooling system

Referring back to Figure 5.5 it can be noted that the total capacity installed in the optimized system exceeds the pick load. This is mainly due to the control strategy employed in the system. The chilled water stored in the tank is always used as much as needed at the beginning of the day. Usually at a certain time the solar radiation drops and no more cooling is available from the absorption chiller. At this time of the day the compression chiller has to entirely satisfy the load and therefore has to have the proper size. This is shown in the lower part of Figure 5.7, where four days of simulation are reported.

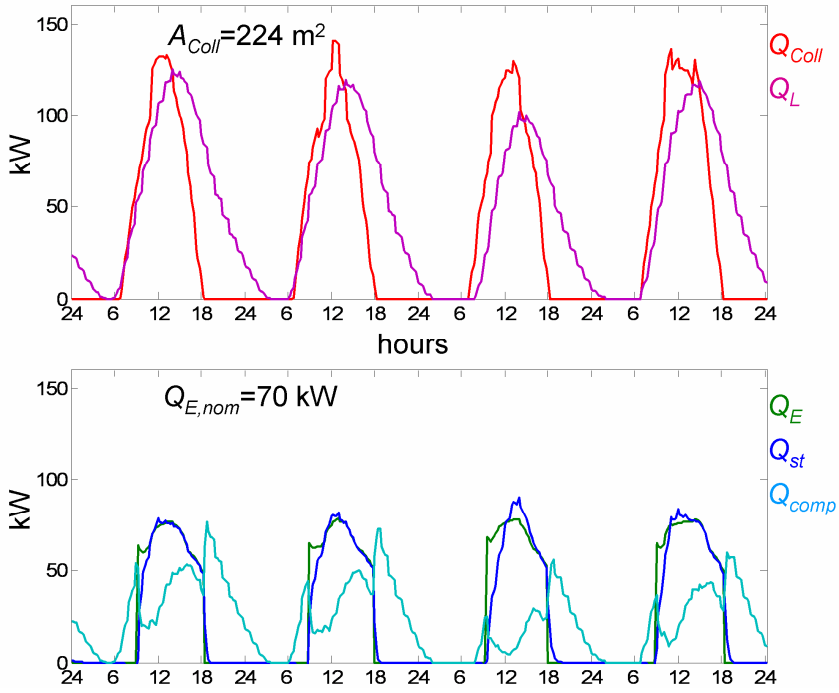

Figure 5.7 Sample of the TRNSYS simulation for a system in Rome. Upper part of the figure shows the thermal energy available from the solar collectors and the loads; lower part of the figure shows the match between cooling power from the absorption chiller, the cold storage and the compression chiller

A different idea can be to provide a base load with the absorption chiller, so that the installed capacity of the compression chiller can be smaller. Care has to be taken in this case to entirely use the chilled water in the tank, since the typical size of the components makes unconvenient to store energy from one day to the other.

5.6.1 Energy performance

The yearly thermal energies exchanged by the two solar cooling systems are shown in Figure 5.8. The consumption of any auxiliary device, like pumps and fan coils, has been neglected in the analysis. Because of the presence of the cold storage not all the energy produced by the absorption chiller is available for cooling purpose. This is for two reasons: first the temperature in the top of the storage can be greater than 12.6 °C (Figure 5.9); as the chiller takes water from the tank and not directly from the load return which is always at 12.6 °C, a quote of the cooling power is not considered to satisfy the load; second losses from the storage take place at all time.

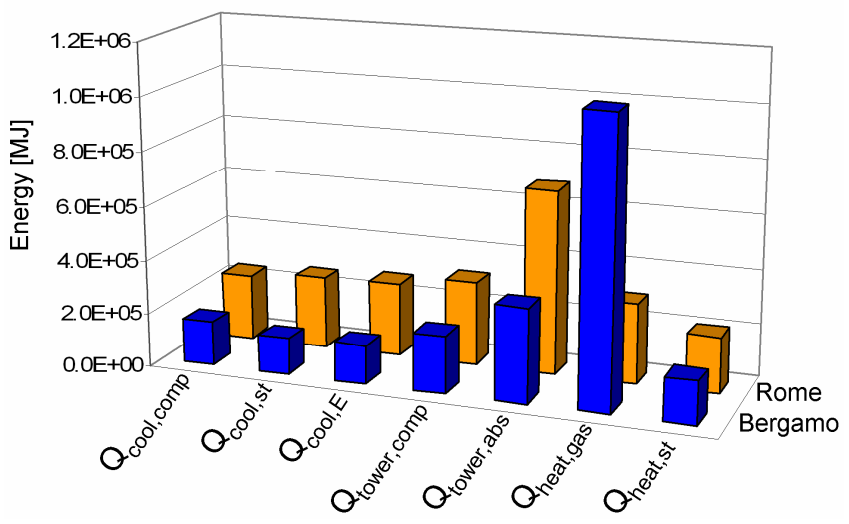

Figure 5.8 Main thermal energies exchanged by the two systems

The definition of the load fraction covered by the absorption chiller is changed to take into account the previous aspect, so *R* is actually the ratio between Q_{st} and Q_L. In Bergamo the value of *R* is equal to 0.45, while in Rome it is 0.52. Figure 5.8 shows how the heat rejection of the absorption chiller is more than two times its cooling energy, while for the compression chiller the thermal energy rejected at the condenser is just a bit more than the cooling capacity.
This issue is reflected by the consumption data, reported in Table 5.4. The avoided electrical consumption, calculated taking the conventional system as a reference, is in Bergamo 7992 kWh. That is the solar cooling system consumes 37 % less electrical energy than the traditional system, while it covers the 45 % of the total load with the solar driven absorption chiller. So, the environmental benefit is always attenuated by the high heat rejection requirement. Of course if a less efficient compression chiller is considered this negative effect has a smaller impact. The same kind of considerations hold for the water consumption, which is really not negligible when wet cooling towers are employed.

Bergamo	Electrical comp [kWh]	Electrical tower comp [kWh]	Electrical tower abs [kWh]	Water tower comp [m^3]	Water tower abs [m^3]	Natural gas [m^3]
Conventional	20056	1367	0	126	0	39148
Solar	11409	763	1259	70	123	33319
Δconsumption	8647	604	-1259	56	-123	5829

Rome	[kWh]	[kWh]	[kWh]	[m^3]	[m^3]	[m^3]
Conventional	35172	2362	0	217	0	16462
Solar	17428	1136	2462	104	232	9354
Δconsumption	17744	1226	-2462	113	-232	7108

Table 5.4 Yearly electrical, water and gas consumption for the reference conventional system and the solar cooling system in the two installation sites

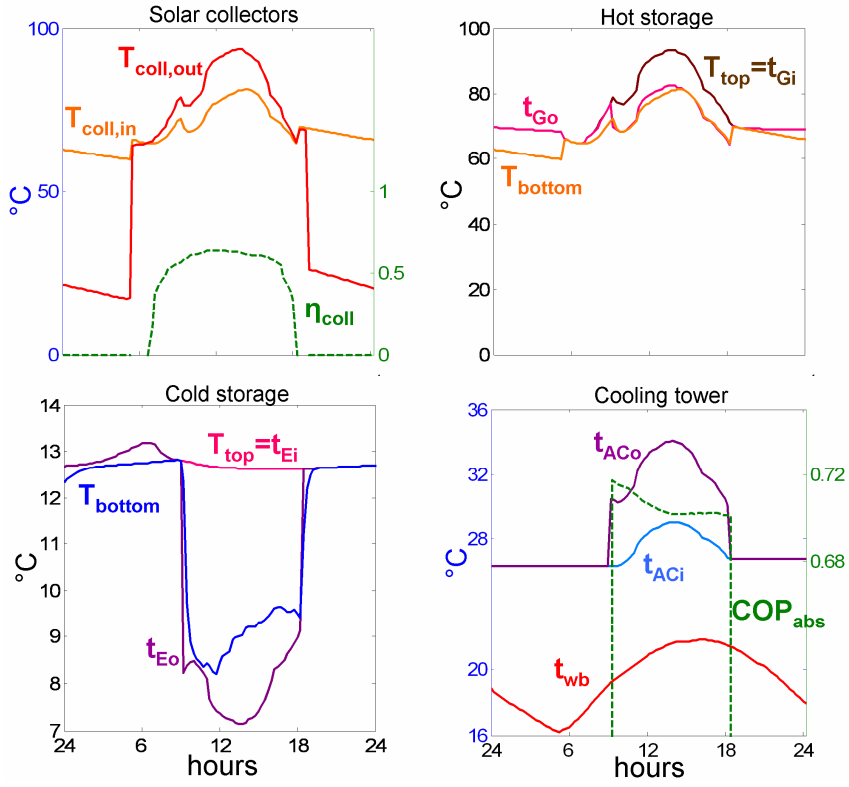

Figure 5.9 Sample of the TRNSYS simulation for a system in Rome. Temperatures of the most relevant components are reported together with the solar collector efficiency in the first figure and the absoption chiller COP in the last figure

5.6.2 Economic evaluation

Two good indicators of economic merit are the solar savings, already defined in chapter 5.4, and the pay back time of the system. The latter is here intended as the number of years needed by the solar system to give a positive value of the solar savings. That is how long do the cumulative savings take to become equal to the difference C_{sol}-C_{conv}. Pay back time plays a central role in the general acceptance of alternative systems. It was

not chosen as the objective of the optimization because this strategy can lead to a minimal employment of solar energy. On the other hand solar savings give the quantity of money effectively saved at the end of the life cycle, so if they are not positive there is no economic motivation to invest in a solar cooling system.
The two cases analysed give both positive solar savings, but only if the italian incentive on collectors purchase is considered. The system in Bergamo has solar savings equal to 25.4 k€, the one in Rome 60.7 k€. It is interesting to note that if half of the collectors cost is not detracted from taxes, like the italian financial law 296/2006 allows, respectively 33 k€ and 40 k€ should be additionally invested in the solar cooling system. So the system in Bergamo would become inconvenient, while still a solar savings of 20 k€ would be possible in Rome. The pay back time is equal to 15 years in Bergamo and 12 years in Rome. More than half of the system life time is needed to get repaid from the additional investment. This prevents certainly the spread of solar cooling technology, unless the investors are highly motivated to purchase renewable cooling equipment. The share of the first costs and of the operation costs in 20 years is reported in Figure 5.10. The operation costs are discounted to a present worth using the figures of Table 5.2.

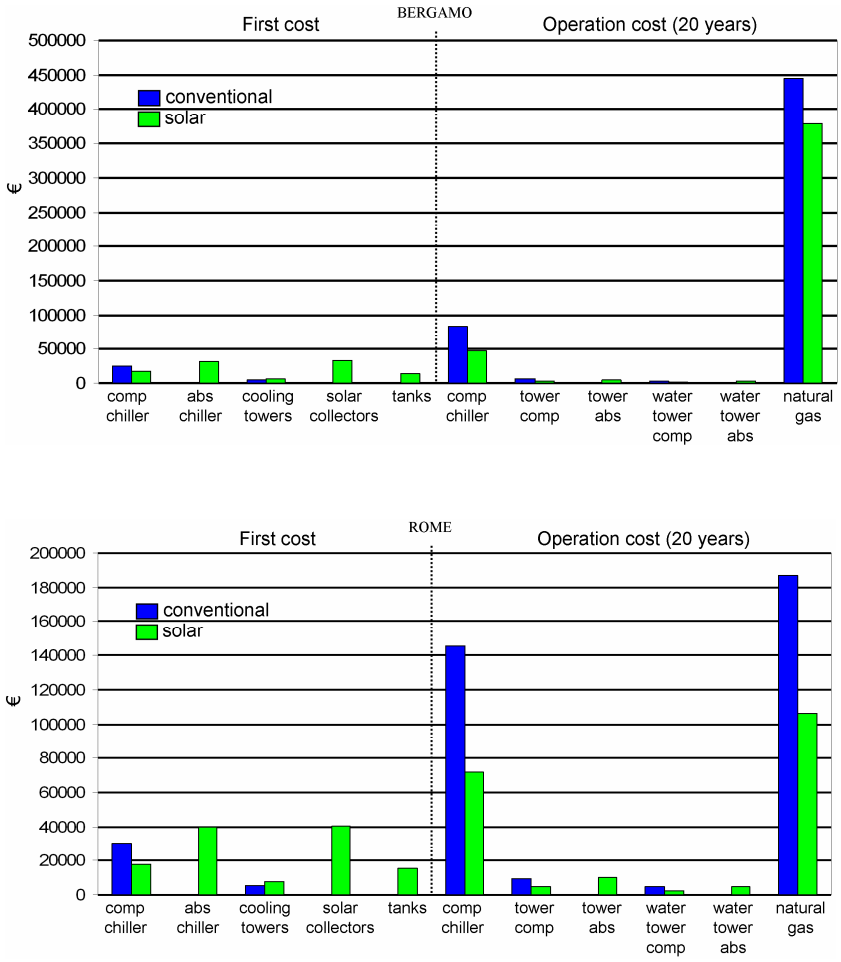

Figure 5.10 Share of the installation first costs and of the operation costs in 20 years

6 Heat exchangers design in a single stage LiBr absorption chiller

The figures employed in the economic analysis of a solar cooling system show that the specific cost of an absorption chiller is much higher than the one of a conventional compression chiller, expecially if small sizes are considered.
The material cost of a chiller is primary based on the heat exchangers of its standard components, the type and number of pumps employed, the purging unit and the control system. Among these items the heat exchangers cost is very sensitive to design choices and is the major part of the investment as the size of the machine increases. Most of the irreversibility that occurs in the cycle is also located in the heat exchangers. The two major sources of entropy generation are the heat transfer process under finite temperature difference and the pressure drop in the flow streams entering the exchangers. So the design of the heat exchangers is a fundamental step of a chiller development.

6.1 Chiller design strategy

Different approaches can be followed in the design of a single stage LiBr machine. Generally an optimum thermodynamic design is not an economic affordable solution, because minimization of irreversibility requires large heat transfer areas and high heat transfer coefficients. Moreover the importance of COP value is strictly correlated to the kind of application the machine is designed for, which determines the price of heat input through the life cycle of the chiller. Under this respect solar cooling is different from trigeneration or district cooling. To restrict the investigation field, chiller design is here addressed for given external circuits temperatures and a given chiller capacity. These fixed conditions are reported in Table 6.1. The advantage of establishing a set of working temperatures is that the COP of a real machine shows its dependency on heat exchangers characteristics and properties of the working fluids, but is allowed to change in a quite narrow range. The degrees of freedom in design choices are presented and discussed in terms of the product UA for every exchanger.

Cooling capacity	5 kW
t_{Ei}	12.5 °C
t_{Eo}	7 °C
t_{Gi}	88 °C
t_{Go}	83 °C
t_{ACi}	31 °C
t_{ACo}	35 °C

Table 6.1 Nominal conditions of the external circuits

6.2 Determination of UA values

The complete set of equations employed in chapter 2.4 to model an absorption chiller can be exploited also in designing a novel chiller. If the nominal working conditions are known, but no information on the heat exchangers is available, the equations allow to find out the product UA for each component of the chiller. This was done in chapter 3 in order to guess the characteristics of the Thermax chiller. What shall be stressed here is that there are infinite combinations of the five UA values that lead to the same performing chiller, that is a chiller working under the conditions reported in Table 6.1 and with a certain COP. This fact opens the possibility to investigate different allocation of the heat transfer area among the components, seeking for an optimized design. Klein [Klein 1991] has described the general problem of optimizing the design of refrigeration cycles, in particular looking for an effective distribution of the heat exchange area between the condenser and the evaporator of a compression chiller. Closely related to the design of absorption chiller, Summerer [Summerer 1995] presented a calculation method to find out the minimum total area and its allocation between the components for different values of COP. Here the goal of finding an optimum design of the absorption chiller is proposed taken into account the area and the geometry of the heat exchangers. Moreover instead of solving the equations simultaneously, like in chapter 2, a parametric study is conducted on four variables, T_E, T_C, x_w and x_s, to see how they influence the UA calculation.

6.2.1 Internal variables effect on the UA calculation

To show how the choice of T_E, T_C, x_w and x_s can influence the final design of the chiller, it is possible to focus on four temperatures differences strictly correlated to them. These are the leaving temperature differences at the evaporator and the absorber: (t_{Eo} – T_E), (T_{Rwi} - t_{ACi}) and the approaching temperature differences at the condenser and the generator: (T_C - t_{ACo}), (t_{Gi} – T_{Rsi}). Assigning a value to the evaporation temperature T_E characterizes the whole evaporator exchanger, because this process occurs at that constant temperature and the external circuit of chilled water is at its design temperatures. Same considerations hold for the condenser and the condensation temperature T_C. In the absorber the leaving temperature difference (T_{Rwi} - t_{ACi}) is determined by the value of T_{Rwi}, which is a function of T_E and x_w. In the generator the approaching temperature difference (t_{Gi} – T_{Rsi}) is determined by the value of T_{Rsi}, which is a function of T_C and x_s. The fact that the solution properties at the absorber and the generator exit are completely defined by the above variables (considering saturated solution), allows to fix some constraints on the values of the weak and strong concentration. On the left hand side of Figure 6.1 are shown different combinations of the evaporation temperature and weak solution concentration, on the right hand side combinations of the condensation temperature and the strong solution concentration. A limit condition occurs for evaporation at 7 °C and x_w = 51.5 %, and for condensation at 35 °C and x_s= 63.6 %, this is the case where all the temperature differences are equal to zero. So the concentration of the solution should always fall between these two values. The two inner curves of Figure 6.1 further show that there are values of the variables for which the two concentrations are very close to each other, in the extreme case their difference can vanish. This is again a constraint on the choice of the variables, because there must be a finite difference between the two concentrations for the absorption cycle to work.

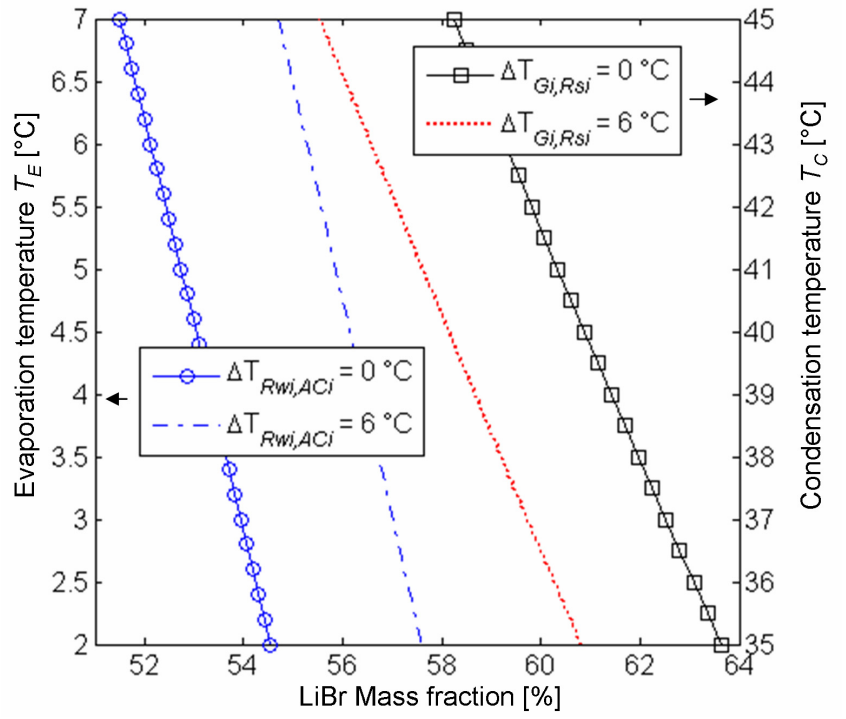

Figure 6.1 Possible values of the variables T_E, T_C, x_w, x_s, and their effect on the temperature differences at the generator ($t_{Gi} - T_{Rsi}$) and at the absorber (T_{Rwi} - t_{ACi})

From Figure 6.1 some other conclusions can be drawn. The size of the evaporator and of the condenser heat exchanger is directly correlated to the choice of evaporation and condensation temperature, increasing as ($t_{Eo} - T_E$) and (T_C - t_{ACo}) approach zero. For the absorber and the generator a prediction of the final size of the exchangers is not so direct, because a part from (T_{Rwi} - t_{ACi}) and ($t_{Gi} - T_{Rsi}$) there are two other temperature differences, respectively ($T_{Rso} - t_{Ci}$) and ($t_{Go} - T_{Rwo}$), that should be calculated with the equations presented in chapter 2.4.

6.3 Heat exchangers design

The type of exchangers employed in each unit and their heat transfer characteristics are presented in this section. This is a critical step of planning a machine and can be rather complex. The prediction of the heat transfer coefficient U is affected by many uncertainties. A great number of parameters have effect on the final performance of the exchangers and unexpected results often arise in practice [Florides et al. 2003, Venegas et al. 2006]. Nevertheless an attempt to use some of the relations available in literature is here made, bearing in mind that the final results depend on the applicability of the correlations considered. All the components employ shell and tubes heat exchangers except the recuperative heat exchanger which is a tube in tube heat exchanger. The solution in the absorber and the generator, as well as the refrigerant in the condenser and evaporator, forms falling film on the tube bundles. All the streams coming from the external circuits flow inside the tubes. The internal heat transfer coefficient h_i for turbulent flows is always calculated with the correlation of Petukhov [Petukhov 1970].

6.3.1 Evaporator heat exchanger

A falling film evaporator with vertical tubes is considered. The present case of a water liquid film evaporating at pressures below 1 kPa was not found in any detail in the available literature. A rough estimate of the heat transfer coefficient h_o is made referring to the work of Chun and Seban [Chun and Seban 1971]. The correlation employed here was developed for water falling in laminar regime with no nucleation. The relation is:

$$h_o = 0.606\, k_l \left(\frac{\mu_l^{\,2}}{\rho_l^{\,2} g} \right)^{-1/3} \left(\frac{\Gamma}{\mu_l} \right)^{-0.22} \tag{6.1}$$

The employment of a recirculation pump is considered to ensure a constant wetting of the tubes.

6.3.4 Condenser heat exchanger

The condenser is designed as a vertical tier of horizontal tubes. The average convection coefficient over N tubes is calculated as in Incropera and De Witt [2002]:

$$h_o = 0.729\left[\frac{g\rho_l(\rho_l-\rho_v)k_l^3 h_{fg}^{'}}{N\mu_l(T_{sat}-T_{wall})D_o}\right]^{1/4} \tag{6.2}$$

6.3.5 Generator heat exchanger

The generator is of the falling film type. A survey on the literature has not produced useful correlations for this specific case of solutes concentration in aqueous solution. A paper from Wang et al. [Wang et al. 1999] describing the experimental operation of a falling film desorber has been employed to have an estimate of the heat transfer coefficient h_o. Nevertheless the mass transfer characteristics of this kind of exchanger depend on a wide range of parameters and in this regard it is not possible to make any prediction for a novel design generator.

6.3.6 Absorber heat exchanger

The design of the absorber is developed following the guidelines of Andberg and Vliet [Andberg and Vliet 1983]. In their paper the authors show a convenient method to determine the total length of a tube bundle needed to obtain a certain outlet concentration for a given inlet concentration and solution mass flow rate. This length is then considered together with the tube diameter to see if the exchanger area is sufficient to release the heat of absorption Q_A. To perform this calculation the heat transfer coefficient h_o is needed. As suggested by Patnaik et al. [1993] Wilke's correlation is used:

$$h_o = \frac{k_{sol}}{\delta}\left(0.029\left(Re_{sol}\right)^{0.53} Pr_{sol}^{0.344}\right) \tag{6.3}$$

$$\delta = \left(\frac{3\mu_{sol}\Gamma}{\rho_{sol}^{\,2} g}\right)^{1/3} \tag{6.4}$$

6.3.7 Recuperative heat exchanger

A tube in tube exchanger is employed for this component of the chiller. The flow is laminar both in the tube and in the annulus. Classical correlations of Kays are employed for the calculation of the convective heat transfer coefficient [Incropera and De Witt 2002].

6.4 Thermodynamic and economic optimization

To perform the optimization a cost function is minimized for different COP values ranging from 0.675 to 0.825. The cost function includes the primary cost of the heat exchangers and the present value of the operating cost of the pumps. The cost of every exchanger is related to the area with the following expression [Boehm 1987]:

$$Z = Z_0 \left(A \right)^n \tag{6.5}$$

The reference cost Z_0 of 1 m^2 is taken equal to 475 €, using data on stainless 304L tubes cost available from a local company. The exponent n is assumed to be 0.9. The cost required to run the pumps of the external circuits is calculated considering an operating time of 720 hours per year and a life expectation of the system of 20 years. The price of the electrical energy is assumed to be 0.2 €/kWh. The power required to drive the pumps is a function of the head loss along the pipes. To calculate the present value of the operating cost an inflation rate of 2% and a discount rate of 5% are respectively assumed. The problem is summarized as:

$$\min \mathrm{P}\left(\overline{y} \right) = \sum_i Z_i \left(\overline{y} \right) + PW_{OPC} \left(\overline{y} \right) \tag{6.6}$$

for a given COP value. The vector $\overline{y}$ is made of the four variables T_E, T_C, x_w, x_s and all the geometric variables used to design the heat exchangers (namely the diameters and the length of tube row for the horizontal bundles).

The results of the optimization are illustrated in Figure 6.2 and reported in Table 6.2. To show how the size of each exchanger changes with the COP the design at COP equal to 0.675 is considered as a reference. As can been

seen the absorber and the recuperative exchanger area generally follow the COP trend. The recuperative heat exchanger, which is often referred as a key element in the determination of the performance, has the highest relative increase of size.

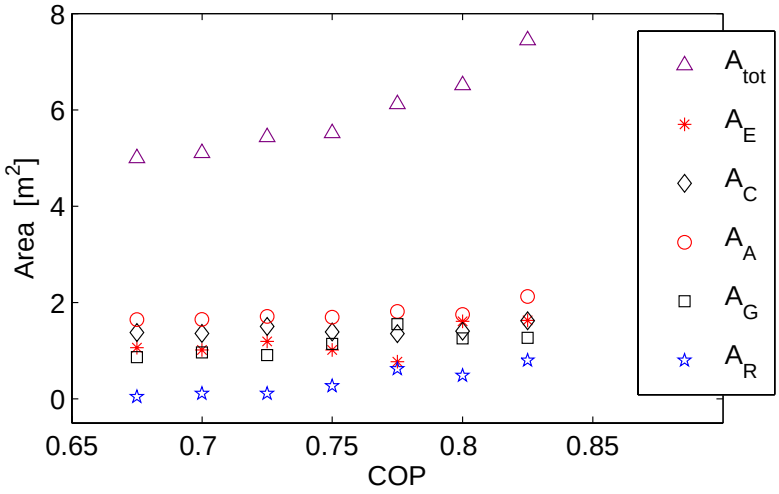

Figure 6.2 Results of the design optimization for COP values between 0.675 and 0.825. The area for each heat exchanger which minimizes the primary and operating cost is reported

For the others components a direct correlation between heat transfer area and performance is not so evident. As described in chapter 6.2 the evaporator and the condenser size are directly correlated to the evaporation temperature T_E and the condensation temperature T_C. The concentration values always fall between the limits depicted in Figure 6.1. The primary cost and the present value of the operating cost are reported in Figure 6.3. The operating price is always a small part of the total cost P.

T_E °C	T_C °C	x_w %	x_s %	A_E m^2	*Incr* %	A_C m^2	*Incr* %	A_A m^2	*Incr* %	A_G m^2	*Incr* %	A_R m^2	*Incr* %
5.61	38.84	54.40	60.81	1.06	0	1.38	0	1.65	0	0.87	0	0.05	0
5.49	38.88	54.50	60.79	1.02	-4	1.36	-1	1.65	+0.2	0.97	+11	0.11	+140
5.92	38.33	53.82	60.99	1.19	+12	1.51	+9	1.72	+4	0.91	+5	0.11	+138
5.48	38.72	54.31	60.84	1.02	-4	1.39	+1	1.70	+3	1.14	+32	0.27	+482
4.46	38.84	54.96	60.88	0.77	-27	1.36	-2	1.82	+10	1.55	+79	0.62	+1239
6.48	38.60	53.41	60.70	1.61	+52	1.41	+2	1.75	+7	1.26	+45	0.48	+939
6.50	37.91	53.16	60.73	1.63	+53	1.62	+18	2.13	+29	1.27	+46	0.80	+1621

Table 6.2 Values of the design variables T_E, T_C, x_w, and x_s resulting from the design optimization. Each row refers to a discrete value of the COP ranging from 0.675 to 0.825, with a 0.25 step. The area of each component is reported with its relative increase or decrease in comparison to the reference size at COP = 0.675

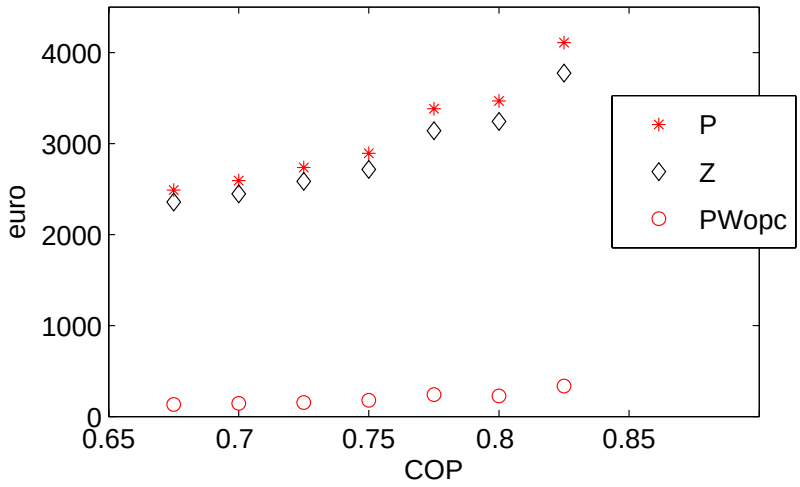

Figure 6.3 Present worth of the operating costs $PW_{opc,}$ primary cost of the heat exchangers Z and total value of the minimised cost function P for different values of the COP

6.5 Conclusions

A numerical procedure has been presented to optimize the design of an absorption chiller. Most of the uncertainties in the final results depend on the unpredictable performance of the heat exchangers. Despite many studies have been devoted in the literature to the heat and mass transfer mechanism in the standard components of the chiller, there is still a lack of reliable correlations for the evaporator and the generator heat exchangers. Further more the recuperative heat exchanger was found to be a critical component in a small size machine, due to the low solution flow rate. In the present study laminar conditions were examined in a tube in tube heat exchanger. Transition flow can be obtained with very small diameters, but head losses become relevant. Other heat exchangers can be considered to replace effectively the tube in tube exchanger.

7 Conclusions and prospect

A model for single stage LiBr-water absorption chillers has been presented. It can be applied to the prediction of the part load behaviour of commercial chillers starting from the knowledge of little information usually available from manufacturers. The results show that the model is able to predict quite well the performance of absorption chillers with mechanical solution pump and refrigerant circulation pump.

The model is then verified against the experimental data of an absorption chiller with thermally driven solution pump and no refrigerant circulation pump at the evaporator. Deviation between the predicted behaviour and real data is found out. This deviation is shown to depend on the different construction characteristics of this type of chillers. An experimental analysis is conducted to develop a more advanced model, that takes into account the variation of the internal flows with the external temperature thrust (t_{Gi}- t_{ACi}) and the off design behaviour of the five heat exchangers. In particular the presence of dry patches in the evaporator tube bundle is seen to strongly influence the capacity of the chiller. Therefore a model of the evaporator tube bundle, which calculates the wetted area of each tube row depending on the refrigerant flow rate, is included in the whole absorption chiller model.

The evolution of the basic model is able to reproduce the characteristic curves of the Yazaki chiller quite well, although further analysis is necessary to better describe the heat and mass transfer processes in the components of the chiller.

The specific problematic of unwetted area in the Yazaki evaporator is usually mitigated in other machines with the use of a recirculation pump. Nevertheless other components like the absorber and the generator might be unable to effectively employ the whole tube area. This is being recognized in other works, where comparison between different heat exchanger performances is investigated. Like for the Yazaki evaporator, the problem reduces to the determination of the exact portion of wetted area in a falling film heat exchanger. Not much more than experimental correlations are available at present to make this kind of calculations, but the argument surely deserves further investigation.

Among the five standard components of the chiller all the heat exchangers have shown to have a variable performance at part load conditions. A part from the absorber, where the variations of the *UA* value were neglected,

experimental correlations have been developed for the generator, the condenser and the regenerative heat exchanger. The solution flow rate is found out to have an influence on both the generator and the regenerative U value.

In the second part of this thesis the design of a solar cooling system is addressed. To guide the design process primary energy savings and economic competitiveness are considered. A configuration that ensures primary energy savings, in comparison with a conventional system based on compression chillers only, includes solar thermal collectors, hot and cold storages, absorption chiller and back up compression chiller. To size the plant elements an optimization-simulation approach is applied. The thermal system is completely defined in the TRNSYS simulation environment. The absorption chiller model is integrated in the TRNSYS standard library. To carry out the optimization the generic tool GenOpt is used. A cost function is evaluated, which depends on the size of the different elements and on the performance of the system, until an optimum value is found.
The procedure applied to a real planning case, considering two different installation sites in Italy, shows that:

1) Sizing of the system must be decided on the basis of all year utilization, with the thermal collectors providing both space heating and cooling
2) The distribution of the thermal loads and of the solar radiation is the most determining factor on the final size of system components.
3) In an alpine climate (Bergamo) the optimized system avoids the use of 45% of conventional energy in summer (compared to a traditional system) and 15% in winter. In a Mediterranean climate (Rome) it leads to save 52% of conventional energy in summer and 43% in winter.
4) The absorption chiller has a considerable heat rejection requirement compared to a modern compression chiller. This fact attenuates the energy savings obtained with solar driven chiller, as electrical energy is employed to run the cooling towers.
5) In the alpine climate there is economic convenience to install a solar cooling system instead of a conventional one only if an incentive on the purchase of solar collectors is considered. The incentive was

introduced in Italy with the financial law 296/2006 and is equal to approximately half the primary cost of the collectors. In the Mediterranean climate also without subsidies there is still a small advantage in purchasing the solar cooling system.

6) Pay back time of the solar cooling system (considering the incentive) ranges from 12 to 15 years. That is the additional investment is repaid in not less than half life cycle, considering 20 years of operation.

To search for the presence of different local maxima in the cost function, additional runs of the optimization have been carried out, changing the bounds on the variables and the algorithm starting point. The investigation has shown that other optimized configurations can be obtained, which actually can gain till 8 % in energy savings, but they do not improve significantly the economic competitiveness of the system. This shows that the method is efficient in determining a good design of the system. Furthermore, due to the flexibility of the TRNSYS environment, any change in the system layout and the effect of different incentives can be easily analysed.

8 References

Albers, J., Ziegler, F. (2003). “Analysis of the part load behaviour of sorption chillers with thermally driven solution pumps”. Proc. of 21st International Congress of Refrigeration, 17-22 August 2003; Washington, USA, Paper ICR0570

Albers, J., Ziegler, F., Asdrubali, F. (2005). “Investigation into the influence of the cooling water temperature on the operating conditions of Thermosyphon Generators”. Proc. of International Sorption Heat Pump Conference, 22.-24. June 2005; Denver, CO, USA, Paper ISHPC-053-2005

Andberg J.W., Vliet G.C., (1983).”Design guidelines for water-lithium bromide absorption refrigerator”. ASHRAE Trans; 89(Part 1B), pp 220-232.

Bohem R.F. (1987). Design analysis of thermal systems. J. Wiley, New York.

Choon N. K. et alii, (2006). “New pool boiling data for water with copper foam metal at sub-atmospheric pressures: Experiments and correlation”. Applied Thermal Engineering, 26, pp. 1286-1290.

Chun K.R., Seban R.A., (1971). “Heat Transfer to Evaporating Liquid Films”. Journal of Heat Transfer; 93, pp 391-396

Duffie J.A., Beckman W.A., (2006). Solar engineering of thermal processes, John Wiley & Sons, New York.

Enke L., (2007). “Bilanzierung der internen Energie- und Stoffströme einer Absorptionskälteanlage mit solarem Antrieb“. Diplomarbeit, Institut für Energietechnik Maschinen - und Energieanlagentechnik, Techinische Universität Berlin.

Florides G.A., Kalogirou S.A., Tassou S.A., Wrobel L.C., (2003). "Design and construction of a LiBr-water absorption machine". Energy Conversion and Management; 44, pp 2483-2508

Franchini G., Nurzia G., Perdichizzi A. (2007), "Renewable cooling with solar assisted absorption chiller: system design". Proceedings of the 62nd National Congress ATI, Salerno.

Grossman G., Michelson E. (1985). "A modular computer simulation of absorption systems". ASHRAE Transactions, Vol.91, Part 2B, pp. 1808-1827

Hellmann H., Grossman G., (1996). "Improved property data correlations of absorption fluids for computer simulation of heat pump cycles". ASHRAE Transactions; 102(1), pp 980-997.

Hellmann H., Schweigler C., Ziegler F. (1998). "A simple method for modeling the operating characteristics of absorption chillers". Seminar EUROTHERM N°59, 6 – 7 July, France.

Hu X., Jacobi, A. M., (1996). ''The Intertube Falling Film Part 1—Flow Characteristics, Mode Transitions and Hysteresis,'' ASME J. Heat Transfer,
118, pp. 616–625.

Incropera F.P., De Witt D.P., (2002). *Fundamentals of Heat and Mass transfer*, 5th ed., John Wiley & Sons.

Klein S.A., (1991). "Design considerations for refrigeration cycles" International Journal of Refrigeration, Vol.15, No. 3, pp. 181-185.

Klein S.A., Alvardo R.L., (1990). "EES: Engineering Equation Solver" F-Chart Software, 4406 Fox Bluff Rd, Middleton, WI 53562.

Klein S.A:, Beckman W.A., Mitchell J.W., Duffie J.A., and others (1996). "TRNSYS – A transient system simulation program" Solar Energy Laboratory, Univ. of Wisconsis, Madison, USA.

Liu Z., Yi J., (2002). “Falling film evaporation heat transfer of water/salt mixtures from roll worked enhanced tubes and tube bundle”. Applied Thermal Engineering, 22, pp. 83-95.
MathWorks (2004). "MATLAB - The language of technical computing." Version 7.0 R14, Math Wors Inc.

Petersen S., Caporal S., Ziegler F. (2006). “Solar cooling-Results of a 10 kW absorption chiller combined with simulated solar thermal systems”. Proceedings of CIERTA International Conference on Renewable Energies and Water Technologies, Almeria.

Petukhov B.S., in Irvine T:F. and Hartnett J.P., Eds., (1970).“Advances in heat transfer”, Vol.6, Academic Press, New York.

Summerer F., (1995). “Evaluation of absorption cycles with respect to COP and economics”. International Journal of Refrigeration, Vol.19, No. 1, pp. 19-24.

Venegas M., Gutierrez G., Roa J., Palacios E., Rodriguez P., (2006). “Thermodynamic characterization of single components in a LiBr-H_2O absorption test rig”. *Proc. of 61st ATI National Congress – International Session “Solar Heating and Cooling”*, Perugia, Italy. pp 111-117.

Wagner W. et alii, (2000). “The IAPWS Industrial Formulation 1997 for the Thermodynamic Properties of Water and Steam”. Transactions of ASME; Vol. 122, pp 150-182.

Wang C., Zhen Lu, Zhou J, (1999). “Enhancement of Heat and Mass Transfer in Lithium Bromide Falling Film Generator”. *Proceedings of the International Sorption Heat Pump Conference*, Munich, Germany. pp 301-305.

Wetter, M. (2004). GenOpt, generic optimization program, user manual, version 2.0.0.Technical Report LBNL-54199, Lawrence Berkeley National Laboratory, Berkeley,CA, USA.

Ziegler F., Albers J., Kuhn A., Petersen S., (2006). “Solar cooling plants: chiller development”. Proceedings of the 61st ATI National Congress, Perugia.